NATIONAL ADVISORY COMMITTEE FOR AERONAUTICS

WARTIME REPORT

ORIGINALLY ISSUED
August 1945 as
Advance Confidential Report L5E04

CHARTS FOR HELICOPTER-PERFORMANCE ESTIMATION

By Herbert W. Talkin

Langley Memorial Aeronautical Laboratory
Langley Field, Va.

NACA

WASHINGTON

NACA ACR No. L5E04

NATIONAL ADVISORY COMMITTEE FOR AERONAUTICS

ADVANCE CONFIDENTIAL REPORT

CHARTS FOR HELICOPTER-PERFORMANCE ESTIMATION

By Herbert W. Talkin

SUMMARY

Charts are presented relating helicopter aerodynamic design variables to performance in steady powered flight. The flight conditions covered are hovering, climb, and horizontal flight. Helicopter speed and lifting rotor power can be found from the charts for known values of fuselage drag coefficient and an average effective blade-element drag coefficient δ. An abbreviated method for estimating δ from the airfoil polar is explained. Although the main emphasis of the report is on relating the design variables to performance, brief consideration is given to the effects of a number of secondary variables, among which are the number of blades, the rotational-energy loss, and the blade shape. An approximate method for estimating the conditions for blade stall is also explained.

The use of the charts is illustrated by numerical examples in order that computations can be made for particular problems.

INTRODUCTION

Existing helicopter aerodynamic-performance theory, like propeller theory, is useful for the correlation of data and the selection of designs. The large number of variables affecting helicopter performance, however, leads to computational difficulties. As in all such cases, computation can be reduced by the use of graphs showing the relations among the essential parameters. In the present paper, equations for such graphs are derived and the use of the resulting charts for performance computation is explained.

The primary purpose of the report is to present, for numerical application, the relations among the aerodynamic design and performance parameters. The actual performance of a given helicopter is influenced by a number of secondary parameters, any one of which has only a small effect on the over-all performance but the quantitative estimation of which presents great difficulties. When the design variables have been selected for a given helicopter, however, it is only by means of the secondary parameters that the efficiency of the helicopter can be improved. For this reason the secondary parameters or efficiency parameters are the proper subject of basic helicopter research. Since the efficiency parameters used herein are for the most part idealized or neglected, the numerical results obtained are considered to be only approximate in absolute value but to give a true representation of the relations among the design parameters. The results should therefore be of practical assistance in comparative performance studies. The accuracy with which the performance must be predicted in a given case will determine the extent to which the efficiency parameters should be investigated. At a number of places in the report secondary parameters have been briefly discussed. Only the following should be considered design parameters:

Y helicopter speed parameter

Y_t blade tip-speed parameter

F rotor-power loading parameter

δ average effective blade-element drag coefficient

C_{D_f} fuselage drag coefficient

σ rotor solidity

The text of this paper is divided, for convenience, into numbered sections. In section 1 a general equation for the aerodynamic performance of helicopters in steady flight is derived from familiar helicopter theory. In sections 2 to 5 the general equation is applied to the construction of graphs for the solution of problems in horizontal flight and climb and the numerical application of the charts is explained. The special problem of the conditions for blade stall in horizontal flight

is considered in section 6. In sections 1 to 6 the problems have been idealized by the use of an average effective blade-element drag coefficient and by neglect of the rotational-energy loss and the loss due to finite-blade number. Methods for estimating these factors are developed in section 7. Finally, in section 8, a numerical example for a typical helicopter is worked out to illustrate the application of the charts and methods developed in the report. The example is so arranged that computations can be made for a given problem without referring to the body of the report. Symbols are defined in the appendix.

1. GENERAL THEORY

A general equation for the aerodynamic performance of helicopters in steady powered flight is derived by a procedure similar to that of reference 1. First, an expression is written for the power required to produce a jet of air through the rotor disk in the absence of blade drag. This power is a function of the inclination of the disk to the air stream. The angle of inclination of the disk is then determined to provide a horizontal component of thrust equal to the component of the total helicopter drag. Next, an expression is obtained for the power increment arising from the rotor torque due to profile drag of the blades. Finally, the total power required for flight is expressed in terms of fundamental parameters.

Part of the rotor power is used for producing a jet of air; the remaining power is used in overcoming the blade profile drag, that is

$$P = P_i + P_\delta \tag{1}$$

where

P rotor power, foot-pounds per second

P_i induced power (rotor power producing thrust)

P_δ power lost in blade drag

Section 1

The power imparted to the thrusting jet is equal to the thrust multiplied by the resultant velocity at the rotor disk in the direction of the thrust. (See fig. 1.)

$$p_i = T(v + V \sin \alpha) \tag{2}$$

where

T rotor axial thrust

v induced axial velocity in the rotor disk

V velocity of the helicopter along its flight path

α angle between rotor disk and flight path

From figure 1 it may be seen that

$$T = \frac{W}{\cos \gamma} + \frac{\rho}{2} V^2 C_{D_f} A \sin \alpha \tag{3}$$

where

W gross weight of the helicopter minus the fuselage lift

γ angle between rotor disk and horizon

A rotor-disk area

ρ mass density of air at altitude

Combining equations (2) and (3) and making use of the relation $\alpha = \alpha_1 + \gamma$ gives

$$p_i = W\left[\frac{v}{\cos \gamma} + V(\sin \alpha_1 + \cos \alpha_1 \tan \gamma)\right] + \frac{\rho}{2} V^2 C_{D_f} A(v + V \sin \alpha) \sin \alpha \tag{4}$$

It will be found convenient to approximate equation (4) by the simpler expression

$$P_i = W\left[v + V(\sin \alpha_1 + \cos \alpha_1 \tan \gamma)\right] + \frac{\rho}{2}V^3 C_{D_f} A \sin^2 \alpha_1 \quad (5)$$

Reference to figure 1 shows that

$$\tan \gamma = \frac{D_h}{W} \quad (6)$$

where

D_h horizontal component of helicopter drag, pounds

In order to obtain a solution for $\tan \gamma$, the contributions of the fuselage and rotor disk may be separated; thus

$$D_h = D_{h_f} + D_{h_s} \quad (7)$$

where D_{h_f} and D_{h_s} apply to the fuselage and rotor disk, respectively.

In deriving an expression for D_{h_s}, several approximations are made, as follows:

(a) The induced velocity is neglected.

(b) The velocity over the blade sections is approximated by the component normal to the blade and in the plane of the disk.

(c) The value of D_{h_s} is approximated by its component in the disk; that is, $\cos \gamma = 1$.

Although these approximations are all optimistic, they are considered to result in a negligible decrease in

the total rotor power required by the helicopter for flight.

For rectangular blades and constant blade-element drag coefficient c_{d_o},

$$D_{h_\delta} \approx \frac{\rho}{4\pi} bcc_{d_o} R \int_0^{2\pi} d\psi \int_0^1 (V \cos \alpha_1 \sin \psi + \Omega R x)^2 \sin \psi \, dx \quad (8)$$

where

b number of blades in rotor disk

c blade chord

ψ angular position of blade in plane of rotation or blade azimuth measured from down-wind position in direction of rotation

Ω rotor angular velocity

R rotor disk radius

x radius ratio $\left(\frac{r}{R}\right)$

r radius to a point on the rotor blade, feet

Integration of equation (8) gives

$$D_{h_\delta} = \frac{\rho}{4} \sigma c_{d_o} \frac{AV^2}{\mu} \cos^2 \alpha_1 \quad (9)$$

where

σ rotor disk solidity $\left(\frac{bc}{\pi R}\right)$

$$\mu = \frac{V \cos \alpha_1}{\Omega R}$$

Also,

$$D_{h_f} = \frac{\rho}{2} C_{D_f} AV^2 \cos \alpha_1 \quad (10)$$

where

C_{D_f} helicopter drag coefficient along flight path, exclusive of rotor blades, based on rotor-disk area A

It follows from equations (6) to (10) and figure 1 that for any steady flight condition

$$\tan \gamma = \frac{\rho_0}{2} Y^2 \left(\frac{\sigma c d_o}{2\mu} \cos \alpha_1 + C_{D_f} \right) \cos \alpha_1 \qquad (11)$$

where ρ_0 is the mass density of air at sea level and Y is the flight-speed parameter,

$$Y = V \sqrt{\frac{A}{W} \frac{\rho}{\rho_0}}$$

On the basis of the approximations made in setting up equation (8), the power (relative to the helicopter) absorbed in the profile drag of the rotor is given by

$$P_\delta \approx \frac{\rho}{4\pi} b c c_{d_o} \Omega R^2 \int_0^{2\pi} d\psi \int_0^1 (V \cos \alpha_1 \sin \psi + \Omega R x)^2 x \, dx$$

Therefore,

$$P_\delta = \frac{\rho}{8} \sigma c_{d_o} A V^3 \frac{1 + \mu^2}{\mu^3} \cos^3 \alpha_1 \qquad (12)$$

The expression for $\tan \gamma$ from equation (11) is substituted in equation (5) to obtain P_i and, with P_δ from equation (12), there is ultimately obtained from equation (1)

$$550F = Y\left(\frac{V}{Y} + \sin \alpha_1\right) + \frac{\rho_0}{2} Y^3 \left[C_{D_f} + \frac{\sigma c_{d_o}}{4\mu^3} (1 + 3\mu^2) \cos^3 \alpha_1 \right] \qquad (13)$$

Section 1

where F is $\frac{P}{W}\sqrt{\frac{A}{W}\frac{\rho}{\rho_0}}$ and is equal to $\frac{1}{550M\sqrt{\rho_0}}$ with M the "figure of merit" of Glauert (reference 2). In terms of thrust and torque coefficients

$$F = 0.0373 \frac{C_Q}{C_T^{3/2}}$$

where

C_Q torque coefficient $\left(\frac{Q}{\rho A(\Omega R)^2}\right)$

C_T thrust coefficient $\left(\frac{T}{\rho A(\Omega R)^2}\right)$

The use of approximation (b) in the derivation of equation (13) results in some error. A more nearly exact analysis not involving assumption (b) has been made in reference 3 from the results of which it is concluded that in equation (13) the coefficient of μ^2 should be approximately 4.6 instead of 3. With this change, and for any blade shape, equation (13) becomes

$$550F = Y\left(\frac{v}{V} + \sin \alpha_1\right) + \frac{\rho_0}{2} Y^3 \left[C_{D_f} + \frac{\sigma\delta}{4\mu^3}(1 + 4.6\mu^2) \cos^3 \alpha_1\right] \quad (14)$$

where

δ rotor-blade average effective profile-drag coefficient (see section 7a)

σ equivalent solidity

$$\left(\sigma = \frac{\int_0^1 \sigma_x x^3 dx}{\int_0^1 x^3 dx} = 4\int_0^1 \sigma_x x^3 dx\right)$$

σ_x solidity at x, $\left(\frac{bc_x}{\pi R}\right)$

The choice of the definition for σ is based on the profile-drag power loss in vertical flight, where it applies

exactly. That σ is also a good approximation for horizontal flight is shown by the negligible effect of blade taper on the stalling limit σY_t^2 in section 6.

An expression for v/V needed for the solution of equation (14) is obtained from the general momentum equation assumed for the thrust of an "actuator disk" in reference 2

$$W \approx T = 2\rho AB^2 vV' \tag{15}$$

in which B has been introduced as a correction for the tip effect due to finite-blade number. Values of B are derived in section 7c. The resultant velocity at the rotor V' is the vector sum of the translational and induced velocities

$$V'^2 \approx (v + V \sin \alpha)^2 + V^2 \cos^2 \alpha \tag{16}$$

Eliminating V' from equations (15) and (16) and making use of the definition $Y = V\sqrt{\frac{A}{W}\frac{\rho}{\rho_0}}$ gives

$$\frac{V}{v} = 2\rho_0 B^2 Y^2 \sqrt{\left(\frac{v}{V}\right)^2 + 2\frac{v}{V}\sin \alpha + 1} \tag{17}$$

2. HORIZONTAL FLIGHT

Derivation.- In horizontal flight, $\cos \alpha_1 = 1$ and equation (14) becomes

$$550F_h = \frac{v_h}{V_h} Y_h + \frac{\rho_0}{2} Y_h^3 \left(c_{D_{f_h}} + \sigma\delta \frac{1 + 4.6\mu^2}{4\mu^3}\right) \tag{18}$$

Values of v_h/V_h in equation (18) may be obtained from equation (17). If $\frac{v_h}{V_h} \sin \alpha$ is considered negligible compared with unity, equation (17) reduces to

$$\frac{V_h}{v_h} = 2\rho_0 B^2 Y_h^2 \sqrt{\left(\frac{v_h}{V_h}\right)^2 + 1} \qquad (19)$$

Numerical application.- In the following explanation of a method for the numerical solution of problems on horizontal flight the application of equation (18) is shown. The power-loading parameter can be expressed as the sum of several contributions which are described, together with graphical means for obtaining them.

The induced power-loading parameter for horizontal flight is given by the first term on the right of equation (18) and is represented by

$$F_{i_h} = \frac{P_{i_h}}{W}\sqrt{\frac{A}{W}\frac{\rho}{\rho_0}}$$

Then,

$$F_{i_h} = \frac{v_h}{V_h}\frac{Y_h}{550} \qquad (20)$$

A plot of F_{i_h} against Y_h obtained from equations (19) and (20) is given in figure 2.

The drag contributions to F_h are given by the last term in equation (18). The total helicopter profile-drag coefficient is represented in this term by the coefficient of $(\rho_0/2)Y_h^3$, which is separated into the part contributed by the rotor blades $\sigma\delta\frac{1 + 4.6\mu^2}{4\mu^3}$ and that due to the rest of the machine $C_{D_{f_h}}$. The fuselage-drag contribution to F_h may be represented by

$$F_{f_h} = \frac{P_f}{W}\sqrt{\frac{A}{W}\frac{\rho}{\rho_0}}$$

where P_f is the horsepower required to overcome fuselage drag. Then, from equation (18),

$$\frac{F_{f_h}}{C_{D_{f_h}}} = \frac{\rho_0}{1100} V_h^3 \tag{21}$$

Equation (21) is plotted in figure 3.

Let the rotor-blade profile-drag contribution to F_h be represented by

$$F_\delta = \frac{P_\delta}{W}\sqrt{\frac{A}{W}\frac{\rho}{\rho_0}}$$

where P_δ is the horsepower loss due to blade profile drag. From equation (18)

$$F_\delta = \frac{\rho_0}{8}\frac{\sigma\delta}{550}\frac{1 + 4.6\mu^2}{\mu^3} V_h^3 \tag{22}$$

Substituting in equation (22) the value $\mu = \frac{V_h}{V_t}$ gives

$$F_\delta = \frac{\rho_0}{8}\frac{\sigma\delta}{550}(1 + 4.6\mu^2)V_t^3$$

or

$$\frac{F_\delta}{\sigma\delta(1 + 4.6\mu^2)} = \frac{\rho_0 V_t^3}{4400} \tag{23}$$

Equation (23) is plotted in figure 4.

It will be recalled that equation (18) has been developed for an actuator disk and therefore does not allow for the rotational-energy loss in the wake of single-rotation rotors nor, with $B = 1$, for the tip loss due to finite-blade number. These small effects are evaluated in sections 7b and 7c, respectively, in terms of F_{rot}, the increase in F due to slipstream rotation, and F_b due to finite-blade number b.

The summation of the contributions to F_h gives, in the order in which they have been explained,

$$F_h = F_{i_h} + F_{f_h} + F_\delta + F_{rot} + F_b \qquad (24)$$

The numerical application of equation (24) is illustrated in section 8b.

The effect of blade shape in equation (24) has been considered only insofar as the plan form affects the value of σ used in calculating F_δ. Blade shape will also have some effect on the induced power-loading terms F_{i_h}, F_{rot}, and F_b.

3. HOVERING AND VERTICAL CLIMB

Derivation.- In vertical climb, $\sin \alpha_1 = 1$ and equation (14) becomes

$$550F_v = \left(\frac{v_v}{V_v} + 1\right) Y_v + \frac{\rho_0}{2} c_{D_{f_v}} Y_v^3 + \frac{\rho_0}{8} \sigma \delta Y_t^3 \qquad (25)$$

Likewise, from equation (17),

$$\frac{v_v}{V_v} = \frac{1}{2}\left(-1 + \sqrt{1 + \frac{2}{\rho_0 B^2 Y_v^2}}\right) \qquad (26)$$

Eliminating v_v/V_v from equations (25) and (26) gives

$$550F_v = \frac{Y_v}{2} + \sqrt{\frac{Y_v^2}{4} + \frac{1}{2\rho_0 B^2}} + \frac{\rho_0}{2} c_{D_{f_v}} Y_v^3 + \frac{\rho_0}{8} \sigma\delta Y_t^3 \qquad (27)$$

The effect of the induced velocity $2v_v$ in increasing the fuselage drag and, therefore, the thrust has not been allowed for in equation (27). This increment in thrust is generally small in hovering and decreases with increasing rate of climb.

Effects of blade plan form and twist.- Equation (27) does not include the effects of blade plan form and twist. When the determination of these effects for a particular blade is desired, element calculations may be made. For that purpose, blade-element formulas are developed herein from the vortex theory of reference 4. The small rotational interference factor a' will be neglected and the rotational-energy loss will be covered in section 7b. Then, from reference 4, in the notation of the present paper and with $a' = 0$,

$$\frac{dC_T}{dx} = \frac{\sigma_x x^2}{2} \left(c_{l_x} \cos \phi - c_{d_o} \sin \phi \right) \sec^2 \phi \qquad (28)$$

and

$$\frac{dC_Q}{dx} = \frac{\sigma_x x^3}{2} \left(c_{l_x} \sin \phi + c_{d_o} \cos \phi \right) \sec^2 \phi \qquad (29)$$

Also,

$$c_{l_x} \cos \phi - c_{d_o} \sin \phi = \frac{v_v + V_v}{1 + v_v + V_v} \frac{8x \sin^2 \phi}{\sigma_x} \qquad (30)$$

where

$$1 + v_v + V_v = \frac{\Omega R x \tan \phi}{V_v} \tag{31}$$

and

$$c_{l_x} = a(\theta_x - \phi) \tag{32}$$

For small values of ϕ, these equations become approximately

$$\frac{dC_T}{dx} = \frac{\sigma_x x^2}{2} c_{l_x} \tag{33}$$

$$\frac{dC_Q}{dx} = \frac{\sigma_x x^3}{2} \left(c_{l_x}\phi + c_{d_o}\right) \tag{34}$$

$$c_{l_x} = \frac{v_v + V_v}{1 + v_v + V_v} \frac{\delta_x \phi^2}{\sigma_x} \tag{35}$$

where

$$1 + v_v + V_v = \frac{\Omega R x}{V_v} \phi \tag{36}$$

and equation (32) remains unchanged; then

$$c_{l_x} = a(\theta_x - \phi)$$

Eliminating $v_v + V_v$ from equations (35) and (36) gives

$$\phi^2 = \frac{\sigma_x c_{l_x}}{\delta_x} \frac{\Omega R x \phi}{\Omega R x \phi - V_v} \tag{37}$$

For hovering $V_v = 0$ and from equation (37)

$$\phi = \frac{1}{2}\sqrt{\frac{\sigma_x c_{l_x}}{2x}} \tag{38}$$

Solving for c_{l_x} from equations (32) and (38) gives

$$c_{l_x} = \frac{3}{4}\left[8\theta_x + 3\frac{\sigma_x}{x} - \sqrt{3\frac{\sigma_x}{x}\left(16\theta_x + 3\frac{\sigma_x}{x}\right)}\right] \tag{39}$$

Also, substituting equation (38) in equation (34) gives

$$\frac{dC_Q}{dx} = \frac{x^3}{2}\left[x\left(\frac{\sigma_x c_{l_x}}{2x}\right)^{3/2} + \sigma_x c_{d_o}\right] \tag{40}$$

For blade-element calculations in vertical climb, equations (32), (33), (34), and (38) apply and in hovering, equations (33), (39), and (40). Graphical integration over the rotor radius gives C_T and C_Q, which are related to the tip-speed parameter and power-loading parameter used herein as follows:

$$Y_t = \sqrt{\frac{1}{\rho_0 C_T}} \tag{41}$$

$$F = \rho_0 C_Q Y_t^3 \tag{42}$$

In the application of the vortex theory it should be remembered that the results obtained are subject to such errors as arise from the assumption of independence of blade elements on which the theory is based. This assumption is believed to be satisfactory for the low rates of axial advance and light disk loadings at which helicopters operate.

Section 3

Numerical application.- As in the case of horizontal flight explained in section 2, the power-loading parameter in vertical flight can be expressed as the sum of several contributions, which are described in this section, together with graphical means for obtaining them.

The induced power-loading parameter for vertical flight is represented by

$$F_{i_v} = \frac{P_{i_v}}{W}\sqrt{\frac{A}{W}\frac{\rho}{\rho_0}}$$

The quantity F_{i_v} is given in equation (27) by the sum of the terms independent of δ. Then,

$$1100F_{i_v} = Y_v + \sqrt{Y_v^2 + \frac{2}{\rho_0 B^2}} + \rho_0 C_{D_{f_v}} Y_v^3 \qquad (43)$$

With $B = 1$, equation (43) gives the induced power-loading parameter F_{i_v} for an actuator disk in vertical flight. The quantity F_{i_v} from equation (43) is plotted against Y_v in figure 5 for several values of $C_{D_{f_v}}$. Calculations made for untwisted rectangular blades by means of the blade-element equations (33) to (40) show an increase in F_{i_v} of approximately 6 percent. It is therefore suggested in figure 5 that, for untwisted rectangular blades, values of F_{i_v} obtained from the curves be increased by 6 percent.

It will be noted from equation (27) that the profile-drag contribution to F_v is given by equation (23) with $\mu = 0$; that is,

$$\frac{F_\delta}{\sigma\delta} = \frac{\rho_0 Y_t^3}{4400} \qquad (44)$$

Values of F_δ may be obtained for known values of Y_t and $\sigma\delta$ from figure 4 with $\mu = 0$.

Equation (27) has been developed for an actuator disk and does not, therefore, allow for the rotational-energy loss in the wake of single-rotation rotors nor, with $B = 1$, for the tip loss due to finite-blade number. These small effects are evaluated in sections 7b and 7c, respectively, in terms of F_{rot} (the increase in F due to slipstream rotation) and F_b due to finite-blade number.

The summation of the contributions to F_v gives, in the order in which they have been explained,

$$F_v = F_{i_v} + F_\delta + F_{rot} + F_b \qquad (45)$$

The numerical application of equation (45) is illustrated in section 8a.

4. CLIMB

Derivation.- The rate-of-climb parameter is defined as

$$Y_c = Y \sin \alpha_1 \qquad (46)$$

For known values of Y and α_1 the power-loading parameter F corresponding to Y_c is given by equation (14). When the power-loading parameter is known, however, the rate-of-climb parameter may be obtained conveniently as a function of the difference between the power-loading parameters required in climb and in horizontal flight at the same values of Y and of C_{D_f}. Such a relation can be obtained by subtracting equation (18) from equation (14). Before the subtraction is made, it is necessary to substitute $\mu = \frac{Y \cos \alpha_1}{Y_t}$ in equation (14) and $\mu = \frac{Y}{Y_t}$ in equation (18). The result is

$$550(F - F_h) = Y_c + \left(\frac{v}{V} - \frac{v_h}{V_h}\right)Y + 1.15\sigma\delta Y_t Y_c^2 \qquad (47)$$

In equation (47) the last term is considered negligible for normal values of $\sigma\delta$ and the equation may be used as

$$550(F - F_h) = Y_c + \left(\frac{v}{V} - \frac{v_h}{V_h}\right)Y \qquad (48)$$

The coefficient of Y in equation (48) is also small and may be satisfactorily computed from equation (17) with $\sin\alpha = \sin\alpha_1$. The physical significance of equation (48) is simply that the excess power required for climb over that required for horizontal flight at the same speed and drag coefficient C_{D_f} is equal to the power necessary to raise the gross weight of the helicopter W plus a small correction for the changed induced loss.

Numerical application.- Equation (48) is plotted in figure 6 for several values of Y. Use of figure 6 to find the rate of climb at any climbing speed necessitates first that a value be found for F_h (section 2), which is the power-loading parameter for the horizontal-speed parameter Y_h equal to the climbing-speed parameter Y. Then, with the known value of $F = \frac{P}{W}\sqrt{\frac{A}{W}\frac{\rho}{\rho_0}}$, calculate $F - F_h$ and read Y_c from figure 6, interpolating to the known value of Y. A numerical example is worked out in section 8e.

5. SPEED FOR MAXIMUM RATE OF CLIMB AND FOR MINIMUM POWER

Derivation.- It is approximated that the best climbing speed is equal to the horizontal speed for minimum power. The condition for minimum power is the same as for minimum F_h with fixed $\frac{W}{A}\frac{\rho_0}{\rho}$ and fixed tip speed ΩR. From

equation (18),

$$550 \frac{dF_h}{dV_h} = \frac{d}{dV_h}\left(\frac{v_h}{V_h} V_h\right) + \frac{3}{2}\rho_0 C_{D_f} V_h^3 + 1.15\rho_0 \sigma\delta V_t V_h = 0 \quad (49)$$

and, from equation (19),

$$\frac{d}{dV_h}\left(\frac{v_h}{V_h} V_h\right) = \frac{-v_h/V_h}{1 + 2(v_h/V_h)^2} \quad (50)$$

The condition for maximum power loading found by substituting equation (50) in equation (49) is

$$1.15\rho_0 V_{best}\left(\sigma\delta V_t + 1.3 V_{best} C_{D_f}\right) = \frac{v_h/V_h}{1 + 2(v_h/V_h)^2} \quad (51)$$

where v_h/V_h is given by equation (19) and V_{best} is the value of $V_h = V \sqrt{\frac{A}{W}\frac{\rho}{\rho_0}}$ for minimum F_h.

Figure 7 is a nomograph for the solution of equation (51). The figure was constructed as follows: At $V_{best} = 0$ a vertical scale of $\sigma\delta V_t$ was laid off. At $V_{best} = 153$ another ordinate of

$$\sigma\delta V_t + 1.3(153)C_{D_f} \equiv \sigma\delta V_t + 200 C_{D_f}$$

was constructed in the same units. Equation (51) was then plotted on these scales with the ordinate representing $\sigma\delta V_t + 1.3 V_{best} C_{D_f}$. The solution for V_{best} is at the intersection of the curve (solid line) with

a straight line (see sample long-dash line) from the value of $\sigma\delta Y_t$ on the left-hand scale to the value of $\sigma\delta Y_t + 200C_{D_f}$ on the right-hand scale. In order to extend the range of the vertical scale, a second curve of equation (51) has been drawn (short dash) based on ordinates ten times as large as the vertical-scale values shown in the figure. The use of figure 7 is explained in more detail on the page facing the figure.

Numerical application.- In order to calculate the maximum value of the rate-of-climb parameter Y_c it is necessary first to find the best climbing-speed parameter Y_{best} and the corresponding power-loading parameter F_h. Values of Y_{best} can be found by means of figure 7. The corresponding value of F_h is obtained from section 2 for $Y_h = Y_{best}$. The value of Y_c can now be determined from section 4 and figure 6. A numerical example is worked out in section 8d.

6. STALLING LIMIT IN HORIZONTAL FLIGHT

Derivation.- Stalling will occur first at the tip of the retreating blade of a rotor in horizontal flight. This stalling is considered a limiting condition for satisfactory performance in respect to vibration, control, and efficiency. In this section, the stalling limit is determined for rotor blades with linear twist and taper with the assumption of uniform axial inflow velocity v_h and without blade coning.

The analysis is similar to that of reference 2 with the following changes:

(a) The disk is tipped through the angle γ_h to provide the horizontal force required for flight in addition to the angle v_h/V_h (see equation (19)) representing the effect of uniform induced inflow

(b) Blades with linear taper and twist are included

The elemental thrust of the rotor disk in horizontal flight may be expressed as

$$\frac{d^2T}{dx\ d\psi} = \frac{bc_x}{2\pi} Ra(\theta_x - \phi)\frac{\rho}{2} V''^2 \qquad (52)$$

where

$$V'' = \Omega R(x + \mu \sin \psi) \qquad (53)$$

Also,

$$\phi = \frac{\lambda/\mu}{\frac{x}{\mu} + \sin \psi} \qquad (54)$$

where λ/μ is the angle between the rotor disk and the resultant velocity

$$\frac{\lambda}{\mu} = \frac{v_h}{V_h} + \gamma_h \qquad (55)$$

Blade taper is represented by the relation

$$c_x = \left[k + x(1 - k)\right] c_t \qquad (56)$$

where k is the blade linear taper ratio. The blade-pitch angle at any point on the disk is given by

$$\theta_x = \theta_t + \theta_1(1 - x) - \theta_2 \sin \psi \qquad (57)$$

where θ_1 is the angle of linear twist and θ_2 is the amplitude of harmonic pitch control.

The thrust coefficient is then obtained by substituting equations (53) to (57) in equation (52) and making use of the definition of σ; thus,

$$\sigma = 4\int_0^1 \sigma_x x^3 \, dx$$

$$\sigma_x = \frac{bc_x}{\pi R}$$

Then

$$\frac{4c_T}{\sigma a}\int_0^1 (k + x - kx)x^3 \, dx =$$

$$\frac{1}{4\pi}\int_0^{2\pi} d\psi \int_0^1 (k+x-kx)(x+\mu \sin \psi)^2 \left[\theta_t + \theta_1(1-x) - \theta_2 \sin\psi - \frac{\lambda}{x+\mu \sin \psi}\right] dx \tag{58}$$

Performing the indicated integrations yields

$$\frac{c_T}{\sigma a}\frac{4+k}{5} = \frac{\theta_1}{24}\left[\frac{3+2k}{5} + (1+2k)\mu^2\right] + \frac{\theta_t}{24}\left[3 + k + 3(1+k)\mu^2\right]$$

$$- \frac{2+k}{12}\left(\theta_2 + \frac{\lambda}{\mu}\right)\mu \tag{59}$$

The amplitude of cyclic pitch control θ_2 is determined by the condition for zero rolling moment on the disk:

$$\int_0^{2\pi} d\psi \int_0^1 x \frac{dc_T}{dx\, d\psi} \sin \psi \, dx = 0 \tag{60}$$

The result is

$$\theta_2 = \frac{4}{3\mu} \frac{(3 + 2k)\theta_1 + 5(3 + k)\theta_t - 5(2 + k)\lambda}{2(4 + k) + 5(2 + k)\mu^2} \tag{61}$$

The lift coefficient at the tip of the blade is given by

$$c_{l_t} = a\left(\theta_t - \theta_2 \sin \psi - \phi\right)$$

$$c_{l_t} = a\left(\theta_t - \theta_2 \sin \psi - \frac{\lambda}{1 + \mu \sin \psi}\right) \tag{62}$$

For the retreating blade, $\psi = \frac{3\pi}{2}$ and

$$c_{l_t} = a\left(\theta_t + \theta_2 - \frac{\lambda}{1 - \mu}\right) \tag{63}$$

By means of equations (59), (61), and (63), values of $\sigma Y_t^2 \left(= \frac{\sigma}{\rho_0 C_T}\right)$ may be calculated for given values of λ/μ and μ when c_{l_t}, a, θ_1, and k have been selected. For the values $c_{l_t} = 1.5$ and $a = 6$, curves of σY_t^2 against λ/μ for several values of μ are plotted on the upper part of figure 8 with $\theta_1 = 0$ and $k = 1$, that is, for untwisted rectangular blades. The arbitrary choice of the conditions $c_{l_t} = 1.5$ and $a = 6$ involves fundamentally the choice of an absolute angle of stall

$$\frac{c_{l_t}}{a} = \frac{1.5}{6} = 0.25 \text{ radian}$$

for use in equation (63) and of the value $a = 6$ as the coefficient of σ in equation (59). Accordingly, the results obtained apply to all values of a for which $\frac{c_{l_t}}{a} = 0.25$, provided that the value obtained for σ is multiplied by $6/a$. The effect of linear twist is illustrated in figure 9 where $\sigma Y_t^2/1000$ is plotted against the linear twist θ_1 for $\mu = 0.3$ and $\frac{\lambda}{\mu} = 0.1$. Taper is shown in figure 10 to have a negligible effect on the stalling limit over the range of taper ratio shown.

In order to use the stalling-limit curves in figure 8, it is necessary to find λ/μ for each operating condition. From equations (11), (19), and (55),

$$\frac{\lambda}{\mu} \approx \frac{1}{2\rho_0 B^2 Y_h^2} + \frac{\rho_0 Y_h^2}{4}\left(\frac{\sigma\delta}{\mu} + 2c_{D_{f_h}}\right) \qquad (64)$$

In the lower part of figure 8, Y_h is plotted against λ/μ for a range of values of $\left(\frac{\sigma\delta}{\mu} + 2c_{D_{f_h}}\right)$ with $B = 1$.

Numerical application.- In order to calculate the stalling limit σY_t^2 it is necessary first to find the value of λ/μ. This value may be determined by means of the set of curves in the lower part of figure 8 for a given value of $\frac{\sigma\delta}{\mu} + 2c_{D_{f_h}}$. The stalling limit σY_t^2 is then read from the upper part of the figure for the given value of μ. The value of σ corresponding to the stalling limit σY_t^2 may be compared with the known value of σ to find whether the given solidity is greater or less than that required for a maximum lift coefficient on the rotor blade (at the tip of the retreating blade) of 1.5. The value of the stalling limit σY_t^2 corresponding to a given Y_t may also be obtained by making successive approximations to σ.

Figure 8 is for untwisted rectangular blades. In order to find stalling limits at angles of attack other than 0.25 radian and for blades with linear twist and taper, charts similar to that of the upper part of figure 8 can be plotted from equations (59), (61), and (63). A numerical example illustrating the use of the charts is worked out in section 8c.

It should be noted that figure 8 has been constructed for zero coning angle. The effects of coning are discussed in reference 5, where coning is shown to increase the lift coefficient at the tip of the retreating blade. A similar effect of blade radial curvature is shown in reference 6. Thus, when figure 8 is applied to actual coning blades, the stalling angle of attack is somewhat higher than the value of 0.25 radian for which the figure was made. Reference 5 also corrects the angle of attack at the blade tip for the average tip-loss factor B by assuming that the disk loading is effectively increased by $1/B^2$. The correction for tip effects on the retreating blade is not known, however, and is probably considerably different from the average correction for the disk. As a result of these blade-deflection and tip effects, the method that has been presented herein for determining the tip-stalling limit does not specify the actual angle of attack at which the tip will stall. The chief value of charts like figure 8 should be in correlating the incidence of stall with helicopter design parameters and operating conditions.

7. SUPPLEMENTARY TOPICS

a. Effective Blade Profile-Drag Coefficient δ

Derivation.- A method of calculating the profile-drag power loss of a rotor in forward flight is explained in reference 7. The method involves calculation of the blade-element angles of attack at 360 stations over the rotor disk and graphical integrations along the radius and around the circumference. Reference 7 also presents contour maps of the angles of attack of the rotor-disk blade elements for untwisted rectangular blades. Examination of these contours suggests that some of the work involved in finding the profile-drag power loss may be eliminated by the use of an average effective blade profile-drag coefficient δ, with the approximation that the drag coefficient is constant along the blade

and equal to the value near the tip. This approximation is suggested by the relatively small change with radius of the average angle of attack per revolution indicated by the contour plots of reference 7. Use of the tip-drag coefficients as representative is further suggested by the fact that the drag power loss is predominantly determined by the tip drag coefficients, as is shown by the weighting curves presented in figure 8 of reference 7. The drag power loss is also shown by equation (8) to increase with nearly the cube of the radius for constant blade drag coefficient.

The method presented herein for determining δ is based on approximations suggested by the foregoing considerations. The determination of δ is made first for untwisted rectangular blades neglecting axial inflow, in which case the angle of attack α is constant along the radius but varies with azimuth ψ and tip-speed ratio μ. The effects of inflow and blade shape are then briefly considered. The method consists in calculating values of the blade-element lift coefficient c_l as a function of σY_t^2, μ, and ψ and using c_l to read c_{d_o} from the airfoil polar. The values of c_{d_o} thus obtained are then multiplied by weighting factors and integrated graphically to find δ. In order to find c_l, the value of θ_x is first obtained from equation (57) for $x = 1$

$$\theta_{x=1} = \theta_t - \theta_2 \sin \psi \tag{65}$$

where

$\theta_{x=1}$ blade pitch angle at tip and at azimuth ψ

θ_t blade pitch angle at tip and at azimuth $\psi = 0$

θ_2 amplitude of harmonic pitch control for lateral balance of the rotor

Also, from equation (61), for $\theta_1 = 0$, $k = 1$, and $\frac{\lambda}{\mu} = 0$,

$$\theta_2 = \frac{16\mu\theta_t}{6 + 9\mu^2} \tag{66}$$

where μ is the tip-speed ratio $V_h/\Omega R$.

From equations (65) and (66),

$$\theta_{x=1} = \theta_t \left(1 - \frac{16\mu}{6 + 9\mu^2} \sin \psi \right) \tag{67}$$

Similarly, from equation (59), for $\theta_1 = 0$, $k = 1$, and $\frac{\lambda}{\mu} = 0$,

$$\frac{6}{a} \frac{C_T}{\sigma\theta_t} = \frac{1}{2}(2 + 3\mu^2) - \frac{8\mu^2}{2 + 3\mu^2} \tag{68}$$

Substituting for θ_t from equation (67) with $\theta_x = \frac{c_l}{a}$ and $C_T = \frac{1}{\rho_0 Y_t^2}$ results in

$$\sigma c_l Y_t^2 = \frac{12}{\rho_0} \frac{2 + 3\mu^2 - \frac{16}{3}\mu \sin \psi}{(2 + 3\mu^2)^2 - 16\mu^2} \tag{69}$$

Curves of $\sigma c_l Y_t^2/1000$ from equation (69) are plotted against $\frac{\psi}{\pi} - \frac{1}{2}$ in figure 11 for a range of values of μ.

The weighting factor will be obtained as

$$\text{W.F.} = \frac{2\pi}{p_\delta + V_h D_{h_\delta}} \frac{d}{d\psi} \left(p_\delta + V_h D_{h_\delta} \right) \tag{70}$$

where p_δ and D_{h_δ} are given in section 1. The result of performing the differentiation indicated in equation (70) is then

$$W.F. = \frac{(\mu \sin \psi + 1)^4 - (\mu \sin \psi)^4}{1 + 3\mu^2} \tag{71}$$

The value of δ may be obtained graphically as

$$\delta = \frac{1}{\pi}\int_{\frac{\pi}{2}}^{\frac{3}{2}\pi} (W.F.)c_{d_o} d\psi$$

$$= \int_0^1 (W.F.)c_{d_o} d\left(\frac{\psi}{\pi} - \frac{1}{2}\right) \tag{72}$$

In the upper part of figure 11, W.F. is plotted against $\frac{\psi}{\pi} - \frac{1}{2}$ for several values of μ.

Numerical application.- The curves of $\sigma c_l Y_t^2/1000$ in figure 11 are used to calculate values of c_l for a number of values of $\frac{\psi}{\pi} - \frac{1}{2}$ ranging from 0 to 1. The corresponding values of c_{d_o} from the blade airfoil-profile polar (see, for example, fig. 12) are then multiplied by the weighting factors W.F. read from figure 11. The products $(W.F.)c_{d_o}$ are plotted against $\frac{\psi}{\pi} - \frac{1}{2}$ and the value of δ is given by the area under the resulting curve. Such a curve is shown in figure 13 (solid line). For blades with section profile varying along the radius, it is suggested that the polar for the section at $x = 0.8$ be used. The use of figure 11 is further explained on the page facing the figure.

Blade twist and the flow through the disk will affect the value of δ. These effects become exaggerated when the blade loading is sufficiently high to cause the blade-element lift coefficients to reach the steeply rising portion of the drag-lift curve, that is, when the stalling limit

is approached. In such cases a more satisfactory approximation to δ will be obtained by including the effect of inflow. Figure 8 shows the effect of inflow angle, expressed as λ/μ, on the stalling limit σY_t^2 for constant μ. The values of c_l obtained from figure 11, before being used to obtain values of c_{d_0} from the airfoil-polar curve, should be increased in approximately the same proportion as the rise in the stalling-limit curve from $\frac{\lambda}{\mu} = 0$ to the value of λ/μ given by figure 8.

The effects of blade taper and twist on δ could be handled in a similar manner but the determination of these effects is considered outside the scope of this paper.

A numerical example is worked out in section 8.

b. Rotational-Energy Loss

In figure 14, figure 88 of reference 2 is for convenience reproduced in part in terms of the parameters of the present paper. Figure 14 shows the variation of the figure of merit M with C_T in hovering for the condition of approximately constant axial velocity along the radius without profile drag. The "ideal" condition of the actuator disk without slipstream rotation is represented by the horizontal line at $M = \sqrt{2}$. The difference between the two conditions on the graph, therefore, represents the effect of slipstream rotation. The difference can be translated into a correction F_{rot} to be added to the values of F for the actuator disk as used herein.

It is assumed that F_{rot} is proportional to both F_{i_h} and F_{i_v}. In that case, from the definition

$$M = \frac{1}{550F\sqrt{\rho_0}} \qquad (73)$$

it follows that

$$\frac{F_{rot}}{F_i} = 1 - \frac{M}{\sqrt{2}} \tag{74}$$

The effect of μ on the rotational-energy loss is neglected. In addition, the effect of blade shape is left to be determined.

Figure 15 shows the curve of the rotational-energy-loss ratio F_{rot}/F_i plotted against Y_t. The quantity F_{rot} must be added to the values found for F_i to correct for rotational-energy loss.

c. Effect of Number of Blades on Performance

The effective-diameter factor B is given in reference 8 by an expression, which in the symbols of this paper becomes

$$B = 1 - \frac{1.386}{b} \frac{\lambda}{\sqrt{1 + \lambda^2}} \tag{75}$$

For small λ, this equation simplifies to

$$B \approx 1 - 1.355\frac{\lambda}{b} \tag{76}$$

where, for vertical flight,

$$\lambda = \frac{V_v + v_v}{\Omega R}$$

$$= \left(1 + \frac{v_v}{V_v}\right)\frac{Y_v}{Y_t} \tag{77}$$

Solving equations (76) and (77) for bY_t and using the expression (26) for v_v/V_v yield

$$bY_t = 0.678 \frac{Y_v}{1 - B}\left(1 + \sqrt{1 + \frac{2}{\rho_0 Y_v{}^2 B^2}}\right) \tag{78}$$

Curves of B against bY_t for several values of Y_v are shown in figure 16. Also shown in this figure are curves for several values of Y_h. These curves were obtained as follows:

In horizontal flight with $\gamma = 0$

$$\lambda = \frac{v_h}{V_h}\frac{Y_h}{Y_t} \tag{79}$$

From equation (79) and the expression for F_{i_h} (equation (20)),

$$\lambda = 550 \frac{F_{i_h}}{Y_t} \tag{80}$$

and substituting equation (80) in equation (76) gives

$$B \approx 1 - 745 \frac{F_{i_h}}{bY_t} \tag{81}$$

The function F_{i_h} is plotted against Y_h in figure 2 and curves of B against bY_t are plotted in figure 16 for several values of Y_h.

The effect of bY_t on F_v remains to be determined. For convenience, the increase in F due to a finite

number of blades is represented by F_b. Then, from equation (27),

$$F_b = \frac{1}{550}\left(\sqrt{\frac{Y_v^2}{4} + \frac{1}{2\rho_0 B^2}} - \sqrt{\frac{Y_v^2}{4} + \frac{1}{2\rho_0}}\right) \qquad (82)$$

In figure 17 are plotted curves of F_b against bY_t for hovering and vertical climb. Also shown in this figure are curves for several values of Y_h, which were obtained as follows:

From equations (19) and (20),

$$(550F_{i_h})^2\left[(550F_{i_h})^2 + Y_h^2\right] = \frac{1}{4\rho_0^2 B^4} \qquad (83)$$

Then F_b at any Y_h is the difference between F_{i_h} calculated from equation (83) with B from equation (81) and F_{i_h} for $B = 1$ (fig. 2). Curves of F_b against bY_t are plotted for several values of Y_h in figure 17. Although the theory thus applied to horizontal flight was derived only for vertical climb, it is considered satisfactory in view of the smallness of F_b.

For a typical value of $bY_t = 1000$, $F_b = 0.0005$ in hovering or a correction on F_{i_v} of only 2 percent. It follows that but little improvement in aerodynamic performance can result from increasing the number of blades without changing the solidity.

8. EXAMPLE

The method for calculating the performance of helicopters by means of the charts that have been developed herein is illustrated for a conventional

helicopter similar to the Sikorsky YR-4. In these calculations the effect of blade shape is not fully accounted for. The performance characteristics to be determined are:

(a) Power required for hovering

(b) Power required at $\mu = 0.3$ (high-speed condition)

(c) Stalling limit in high speed

(d) Best climbing speed

(e) Maximum rate of climb

The following values are selected as the design specifications:

Gross weight, W, pounds	2550
Fuselage lift	Negligible
Blade shape (see sketch, fig. 18)	Tapered and twisted 7°
Number of blades, b	3
Blade-element profile (conventional rough) Airfoil polar of figure 12 adapted from reference 7	
Rotational tip speed, ΩR, feet per second	480
Blade radius, R, feet	19
Fuselage equivalent flat-plate area in horizontal flight, f_h, square feet	20
Density ratio, ρ/ρ_0	1

From the foregoing values, the following essential quantities are first calculated for subsequent use in the performance calculations:

$$A = 1134$$

$$\frac{W}{A} = 2.25$$

$$C_{D_{f_h}} = \frac{f_h}{A} = 0.0176$$

$$Y_t = \Omega R \sqrt{\frac{A}{W} \frac{\rho}{\rho_0}} = 320$$

and by graphical integration

$$\sigma = 4 \int_0^1 \sigma_x x^3 dx = 0.056$$

a. Power Required for Hovering

The power required for hovering is calculated as the sum of four contributions. The condition of hovering is treated as a limiting case of vertical flight. Expressed in terms of power-loading parameters,

$$F_v = F_\delta + F_{i_v} + F_{rot} + F_b$$

where the contributions are, respectively, due to rotor-blade drag, axial-induced loss, rotational-energy loss, and blade-tip loss due to a finite number of blades. In this example, these contributions will be calculated and totalled.

In order to find F_δ, it is necessary to find δ, the average effective blade profile-drag coefficient. From figure 11, for $\mu = 0$,

$$\sigma c_l Y_t^2 = 2500$$

Therefore,

$$c_l = \frac{2500}{\sigma Y_t^2}$$

$$= \frac{2500}{0.056 \times (320)^2}$$

$$= 0.44$$

From the airfoil polar (see fig. 12)

$$\delta = 0.0122$$

From figure 4 the profile-drag power loss is given in terms of F_δ by

$$\frac{F_\delta}{\sigma\delta} = 17.7$$

Therefore

$$F_\delta = 0.056 \times 0.0122 \times 17.7$$

$$= 0.0121$$

From figure 5 at $Y_v = 0$ read the induced-power-loss term for untwisted rectangular blades

$$F_{i_v} = 0.0264 \times 1.06$$

$$= 0.0280$$

From figure 15 read at $Y_t = 320$,

$$\frac{F_{rot}}{F_i} = 0.0115$$

The rotational-energy-loss term is therefore

$$F_{rot} = 0.0115F_{i_v}$$

$$= 0.0115 \times 0.0280$$

$$= 0.0003$$

From figure 17 read for $Y_v = 0$ at $bY_t = 960$ the blade-tip-loss term $F_b = 0.0006$. Then compute

$$F_v = F_\delta + F_{i_v} + F_{rot} + F_b$$

$$= 0.0121 + 0.0280 + 0.0003 + 0.0006$$

$$= 0.0410$$

From the definition of F_v,

$$F_v = \frac{P_v}{W}\sqrt{\frac{A}{W}\frac{\rho}{\rho_0}}$$

calculate for the given values of A and W

$$P_v = F_v W \sqrt{\frac{W}{A}}$$

$$= 0.0410 \times 2550 \times 1.5$$

$$= 157 \text{ horsepower required to hover}$$

The value thus obtained applies to untwisted rectangular blades. Such a calculation is useful for determining the effects on hovering of all the aerodynamic design variables. When the effects of blade shape are of primary interest, however, blade-element computations may be made by equations (33), (39), and (40) and the thrust and torque coefficients may be found by graphical integration. When this procedure is followed for the given tapered blade with 7° linear twist, it is found that the profile-drag loss is unchanged but $F_{i_v} = 0.0273$; that is, by the short method the induced loss calculated is too large by 3 percent. The power required for hovering is then 154 instead of 157 horsepower.

This comparison does not take into account the change in fuselage down load due to the changed rotor-slipstream velocity distribution. It is noted, however, that improvements in blade design which decrease the induced-power loss must increase the downwash through the central portion of the rotor disk beneath which is generally located the widest part of the fuselage. The resulting increase in fuselage vertical drag tends to reduce the net gain from improved disk loading.

When the effect of blade shape on hovering performance is to be determined, the induced-power-loading term F_{i_v} should be obtained from element calculations but the profile-drag loss as determined from δ is generally satisfactory.

b. Power Required for High Speed

The power required for high-speed horizontal flight is calculated as the sum of five contributions. Expressed in terms of power-loading parameters,

$$F_h = F_\delta + F_{f_h} + F_{i_h} + F_{rot} + F_b$$

where the contributions are due, respectively, to rotor-blade drag, fuselage drag, axial-induced loss, rotational-energy loss, and blade-tip loss due to a finite number of blades. In the example, these contributions will be calculated and totalled.

In order to find F_δ, it is necessary, as in the case of hovering (section 8a), to find δ. From figure 11, for $\mu = 0.3$, read values of $\sigma c_l Y_t^2/1000$ at a number of abscissa stations from $\frac{\psi}{\pi} - \frac{1}{2} = 0$ to 1. For each station calculate c_l by use of the given value of

$$\frac{\sigma Y_t^2}{1000} = \frac{0.056(320)^2}{1000}$$

$$= 5.74$$

For each value of c_l thus obtained, read c_{d_o} from the airfoil polar (fig. 12) and multiply each value of c_{d_o} by the weighting factor W.F. read from the upper set of curves for $\mu = 0.3$. Then plot these products against the abscissa and integrate graphically. The result is δ. For the given blade the curve of $(W.F.)c_{d_o}$ is shown by the solid-line curve in figure 13 and from the area under the curve $\delta = 0.0121$. In the determination of δ in the manner just described, the effect of the inflow through the rotor disk has been neglected to simplify the explanation. When this effect is to be considered, the procedure for finding δ is altered, as explained in section 7a, in the following manner:

Calculate the value of $\frac{\sigma\delta}{\mu} + 2c_{D_{f_h}}$. In this case, the value of δ found for hovering may be conveniently used because the final determination of δ for horizontal flight is relatively insensitive to the approximate value used at this point. Then,

$$\frac{\sigma\delta}{\mu} + 2c_{D_{f_h}} = \left(\frac{0.056 \times 0.0122}{0.3}\right) + (2 \times 0.0176)$$

$$= 0.0375$$

Calculate $Y_h = \mu Y_t = 96$ and then interpolate between the curves of $\frac{\sigma\delta}{\mu} + 2c_{D_{f_h}}$ in the lower part of figure 8 to the value 0.0375 and at $Y_h = 96$, proceed upward to the curve of $\mu = 0.3$ in the upper part of the graph and read the stalling limit $\sigma Y_t^2 = 4270$. For the same curve of μ read also at $\frac{\lambda}{\mu} = 0$, $\sigma Y_t^2 = 3500$. The ratio of these two values of σY_t^2 is now to be used as a factor to increase the values of c_l obtained from the lower part of figure 11. The resulting curve of $(W.F.)c_{d_o}$ is shown dashed in figure 13 and gives the value $\delta = 0.0127$.

From figure 4 read for $Y_t = 320$

$$\frac{F_\delta}{\sigma\delta(1 + 4.6\mu^2)} = 17.7$$

Therefore, the profile-drag power loss is given by

$$F_\delta = 17.7\sigma\delta\left(1 + 4.6\mu^2\right)$$

$$= 17.7 \times 0.056 \times 0.0127 \times (1 + 0.41)$$

$$= 0.0178$$

From figure 3 read, for $Y_h = \mu Y_t = 0.3 \times 320 = 96$, the quantity

$$\frac{F_{f_h}}{C_{D_{f_h}}} = 1.77$$

Therefore,

$$F_{f_h} = 1.77 C_{D_{f_h}}$$

$$= 1.77 \times 0.0176$$

$$= 0.0312$$

From figure 2 read the induced-power loss for $Y_h = 96$

$$F_{i_h} = 0.0040$$

Section 8

From figure 15 read at $Y_t = 320$, $\frac{F_{rot}}{F_i} = 0.0115$ and hence the rotational-energy-loss term is

$$F_{rot} = 0.0115 F_{i_h}$$

$$= 0.0115 \times 0.0040$$

$$= 0.00005$$

which is negligible in comparison with F_h.

From figure 17 for $bY_t = 3 \times 320 = 960$, read for $Y = 0$ the tip-loss term

$$F_b = 0.0006$$

Then, find the sum

$$F_h = F_\delta + F_{f_h} + F_{i_h} + F_{rot} + F_b$$

$$= 0.0178 + 0.0312 + 0.0040 + 0 + 0.0006$$

$$= 0.0536$$

From the definition of F_h,

$$F_h = \frac{P_h}{W} \sqrt{\frac{A}{W} \frac{\rho}{\rho_0}}$$

calculate for the given values of A and W

$$P_h = F_h W \sqrt{\frac{W}{A}}$$

$$= 0.0536 \times 2550 \times 1.5$$

$$= 205 \text{ horsepower}$$

This power is required by the rotor in horizontal flight at $\mu = 0.3$, that is, at 98 miles per hour.

c. Stalling Limit in High Speed

In order to estimate whether a rotor has sufficient solidity to avoid stalling in the high-speed flying condition, the stalling limit is calculated by means of a chart similar to figure 8. The upper part of figure 8 applies only to untwisted rectangular blades. The effects of linear twist and taper are illustrated in figures 9 and 10, respectively, for the condition $\mu = 0.3$ and $\frac{\lambda}{\mu} = 0.1$. Also, graphs similar to the upper part of figure 8 can be constructed for any combination of linear twist and taper by means of equations (59), (61), and (63) developed in section 6. For other blade shapes it may be possible to obtain analytic solutions for the actual blade twist and taper, as was done in section 6 for the linear shapes, or it may be desirable to obtain some experimental points and to fair in curves for an approximately equivalent linear twist and taper.

In the present example, the stalling limit is determined for untwisted blades of the equivalent solidity σ of the blade sketched in figure 18 in order to illustrate the use of the type of chart of figure 8. The procedure follows: Calculate $Y_h = \mu Y_t = 96$. Also, with the value of δ obtained from section 8b for high-speed flight

$$\frac{\sigma\delta}{\mu} = \frac{0.056 \times 0.0127}{0.3}$$

$$= 0.0023$$

$$\frac{\sigma\delta}{\mu} + 2c_{D_{f_h}} = 0.0023 + (2 \times 0.0176)$$

$$= 0.0375$$

Section 8

The stalling limit can now be read from figure 8. Interpolate between the curves of $\frac{\sigma\delta}{\mu} + 2c_{D_{f_h}}$ in this figure to the value 0.0375 and at $Y_h = 96$ proceed upward to the curve $\mu = 0.3$ in the upper part of the graph and read the stalling limit $\sigma Y_t^2 = 4270$. For $Y_t = 320$, $\sigma = 0.042$.

Since this value of σ is some 25 percent smaller than the given value of 0.056, the given blade solidity is sufficiently large to avoid stall. Note that figures 9 and 10 show that the effects of twist and taper are to lower the stalling limit still further. As explained in section 6, figure 8 should be regarded as a means of estimating relative tendency to stall and not as determining the actual operating condition at which stall occurs.

d. Best Climbing Speed

The best-climbing-speed parameter Y_{best} is given in figure 7. In order to use this figure it is necessary to calculate $\sigma\delta Y_t$ in which the value of δ is for horizontal flight at the best climbing speed. The value of $\delta = 0.0122$ obtained for hovering in section 8a may be used satisfactorily because in this example δ varies only slightly with μ and increases to only 0.0127 at $\mu = 0.3$. Then,

$$\sigma\delta Y_t = 0.056 \times 0.0122 \times 320$$

$$= 0.22$$

Also,

$$200c_{D_{f_h}} = 200 \times 0.0176$$

$$= 3.52$$

$$\sigma\delta Y_t + 200c_{D_{f_h}} = 3.74$$

A straight edge is then laid on figure 7 passing through $\frac{\sigma\delta Y_t}{10} = 0.022$ on the left-hand scale and

$\frac{1}{10}\left(\sigma\delta Y_t + 200C_{D_{f_h}}\right) = 0.374$ on the right-hand scale.

The intersection with the dash-line curve is at $Y_{best} = 40.4$. The first approximation to μ is, therefore, $\frac{Y_{best}}{Y_t} = \frac{40.4}{320} = 0.126$. With this value of μ, a second approximation to δ could be calculated for use with figure 7 by the procedure of section 8b but, as in this case, the first approximation is usually sufficient because the increase in δ with μ is small. The best climbing speed is therefore

$$V_{best} = Y_{best}\sqrt{\frac{W}{A}\frac{\rho_0}{\rho}}$$

$$= 40.4\sqrt{2.25}$$

$$= 60.6 \text{ feet per second}$$

$$= 41.3 \text{ miles per hour}$$

e. Maximum Rate of Climb

The rate of climb is obtained from figure 6 and the maximum rate of climb is obtained with $Y = Y_{best}$. From section 8d, $Y_{best} = 40.4$. The value of F_h for $Y_{best} = Y_h = 40.4$ is obtained by a procedure similar to that of section 8b. The result is (on the assumption that $C_{D_f} = C_{D_{f_h}}$)

$$F_h = F_\delta + F_{f_h} + F_{i_h} + F_{rot} + F_b$$

$$= 0.0156 + 0.0026 + 0.0093 + 0 + 0.0006$$

$$= 0.0281$$

Also, if the available rotor power is assumed to be 200 horsepower,

$$F = \frac{P}{W}\sqrt{\frac{A}{W}\frac{\rho}{\rho_0}}$$

$$= \frac{200}{2550\sqrt{2.25}}$$

$$= 0.0523$$

and

$$F - F_h = 0.0523 - 0.0281$$

$$= 0.0242$$

From figure 6, read Y_c for $Y = Y_{best} = 40.4$; $Y_c = 13.5$. The maximum rate of climb is therefore

$$V_c = Y_c\sqrt{\frac{W}{A}\frac{\rho_0}{\rho}}$$

$$= 13.5\sqrt{2.25}$$

$$= 20.25 \text{ feet per second}$$

$$= 1215 \text{ feet per minute}$$

CONCLUDING REMARKS

The relations among the principal helicopter aerodynamic design and performance variables have been expressed in terms of power-loading parameters and speed parameters, both of which are functions of the rotor disk loading. The relations among these parameters have been plotted

for various conditions of steady powered flight to reduce the labor necessary to use them in numerical performance computations. In a concluding numerical example, sample computations, which may be used as a general guide for other calculations, are worked for a conventional type of helicopter.

Langley Memorial Aeronautical Laboratory
National Advisory Committee for Aeronautics
Langley Field, Va.

APPENDIX

SYMBOLS

A	rotor-disk area, sq ft
a	slope of the lift curve $\left(\frac{c_l}{a_r}\right)$
a'	rotational interference factor
B	factor applied to rotor-disk diameter to allow for blade-tip effect due to finite-blade number
b	number of blades in the rotor disk
c	blade chord $\left(c_x = \left[k + x(1 - k)\right]c_t\right)$
C_{D_f}	helicopter drag coefficient along flight path, exclusive of rotor blades, based on rotor-disk area A
c_{d_o}	rotor-blade-element profile-drag coefficient
c_l	rotor-blade-element lift coefficient
C_Q	torque coefficient $\left(\frac{Q}{\rho AR(\Omega R)^2}\right)$
C_T	thrust coefficient $\left(C_T = \frac{T}{\rho A(\Omega R)^2} = \frac{1}{\rho_0 Y_t^2}\right)$
D	helicopter drag, lb
F	power-loading parameter for any flight path $\left(\frac{P}{W}\sqrt{\frac{A}{W}\frac{\rho}{\rho_0}}\right)$
F_b	increase in F due to finite-blade number
F_{rot}	increase in F due to slipstream rotation

f	fuselage equivalent flat-plate area based on unit-drag coefficient, sq ft
k	blade linear taper ratio
M	figure of merit $\left(\frac{1}{550F\sqrt{\rho_0}}\right)$
P	rotor power, horsepower
p	rotor power, ft-lb/sec
Q	rotor torque, lb-ft
R	rotor-disk radius, ft
r	radius to a point on rotor blade, ft
T	rotor axial thrust, lb
v	induced axial velocity in rotor disk, ft/sec (positive downward)
V	velocity of the helicopter along its flight path, ft/sec
V'	resultant wind velocity through the rotor disk, ft/sec
V''	resultant velocity of a rotor blade element, ft/sec
V_c	rate of climb, ft/sec
W	gross weight of the helicopter minus the fuselage lift, lb
W.F.	weighting factor
x	radius ratio $\left(\frac{r}{R}\right)$
Y	helicopter velocity parameter $\left(V\sqrt{\frac{A}{W}\frac{\rho}{\rho_0}}\right)$
Y_c	helicopter rate of climb parameter $\left(V_c\sqrt{\frac{A}{W}\frac{\rho}{\rho_0}}\right)$

Y_{best} value of Y_h for minimum F_h

Y_t rotor tip-speed parameter $\left(\Omega R\sqrt{\frac{A}{W}\frac{\rho}{\rho_0}}\right)$

α_1 angle between flight path and horizon, radians

α angle between rotor disk and flight path, radians

α_r blade-element angle of attack from zero lift, radians

γ angle between rotor disk and horizon, radians

δ rotor-blade average effective profile-drag coefficient

θ_x blade-element pitch angle, radians $\left(\theta_t + \theta_1(1 - x) - \theta_2 \sin\psi\right)$

θ_t blade tip angle at zero azimuth, radians

θ_1 angle of linear twist of the blade, radians

θ_2 amplitude of harmonic pitch control for lateral balance of the rotor, radians

$\lambda = \left(\frac{v}{V} + \sin\alpha\right)\frac{\mu}{\cos\alpha_1}$; $\lambda\Omega R$ is speed of axial flow through rotor disk (positive downward)

μ ratio of the horizontal component of speed of the helicopter to the rotational tip speed of the rotor

$$\left(\mu = \frac{V\cos\alpha_1}{\Omega R} = \frac{Y_h}{Y_t}\right)$$

ρ mass density of air at altitude

ρ_0 mass density of air at sea level (0.002378 slug/cu ft)

σ equivalent solidity $\left(\sigma = \dfrac{\int_0^1 \sigma_x x^3 dx}{\int_0^1 x^3 dx} = 4 \int_0^1 \sigma_x x^3 dx \right)$

$\sigma_x = \dfrac{bc_x}{\pi R}$

ϕ angle of inflow, radians

ψ blade azimuth measured from down-wind position in direction of rotation, radians

Ω rotor angular velocity, radians/sec

Subscripts:

f due to fuselage drag

h for horizontal flight

i induced

t at the blade tip

v for vertical flight

x for the radius ratio $\left(\frac{r}{R} = x\right)$

δ due to blade profile drag

REFERENCES

1. Wald, Quentin: A Method for Rapid Estimation of Helicopter Performance. Jour. Aero. Sci., vol. 10, no. 4, April 1943, pp. 131-135.

2. Glauert, H.: Airplane Propellers. Helicopter Airscrews. Vol. IV of Aerodynamic Theory, div. L, ch. X, W. F. Durand, ed., Julius Springer (Berlin), 1935, pp. 310-324.

3. Bennett, J. A. J.: Rotary-Wing Aircraft. Aircraft Engineering, vol. XII, no. 133, March 1940, pp. 65-67, 79.

4. Glauert, H.: Airplane Propellers. The Vortex Theory. Vol. IV of Aerodynamic Theory, div. L, ch. VI, sec. 1, W. F. Durand ed., Julius Springer (Berlin), 1935, pp. 230-232.

5. Bailey, F. J., Jr: A Simplified Theoretical Method of Determining the Characteristics of a Lifting Rotor in Forward Flight. NACA Rep. No. 716, 1941.

6. Lock, C. N. H.; Further Development of Autogyro Theory. Parts I and II. R. & M. No. 1127, British A.R.C., 1928.

7. Gustafson, F. B.: Effect on Helicopter Performance of Modifications in Profile-Drag Characteristics of Rotor-Blade Airfoil Sections. NACA ACR No. L4H05, 1944.

8. Glauert, H.: Airplane Propellers. Propellers of Highest Efficiency. Vol. IV of Aerodynamic Theory, div. L, ch. VII, sec. 4, W. F. Durand, ed., Julius Springer (Berlin), 1935, pp. 261-266.

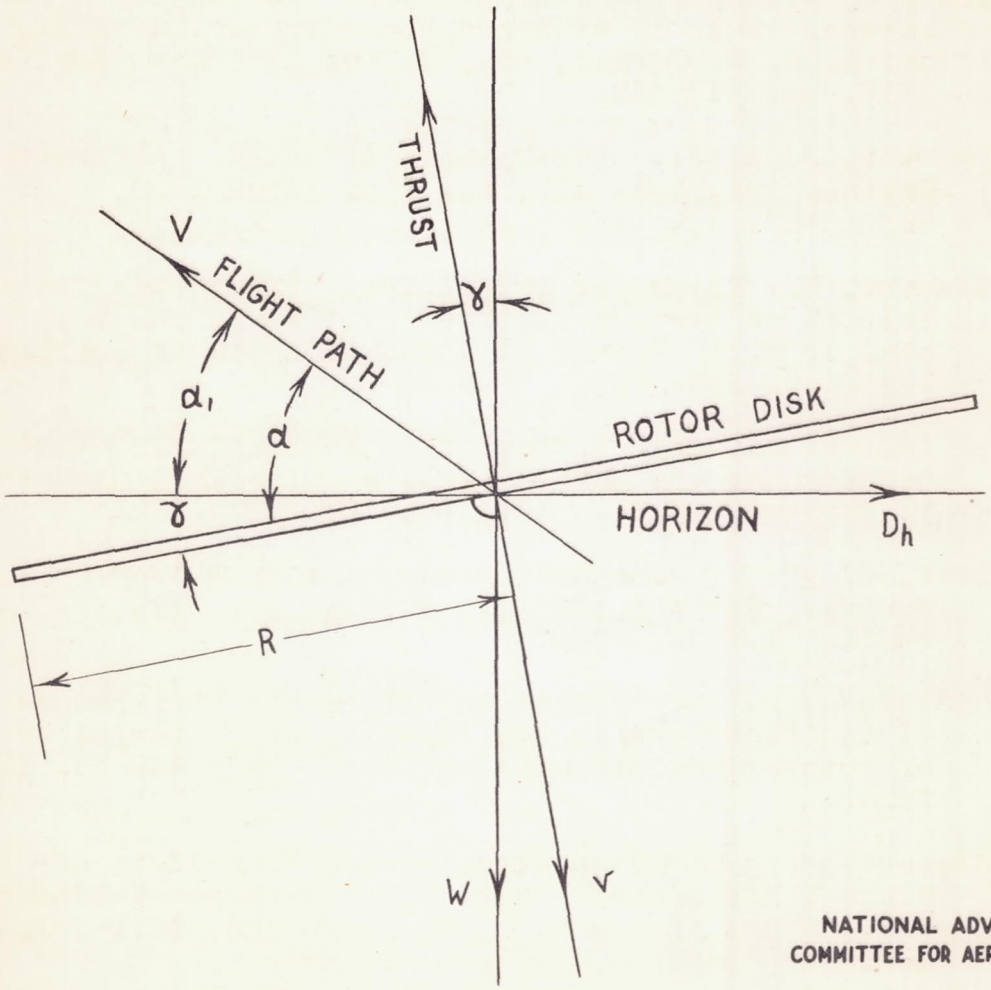

Figure 1.- Rotor geometry.

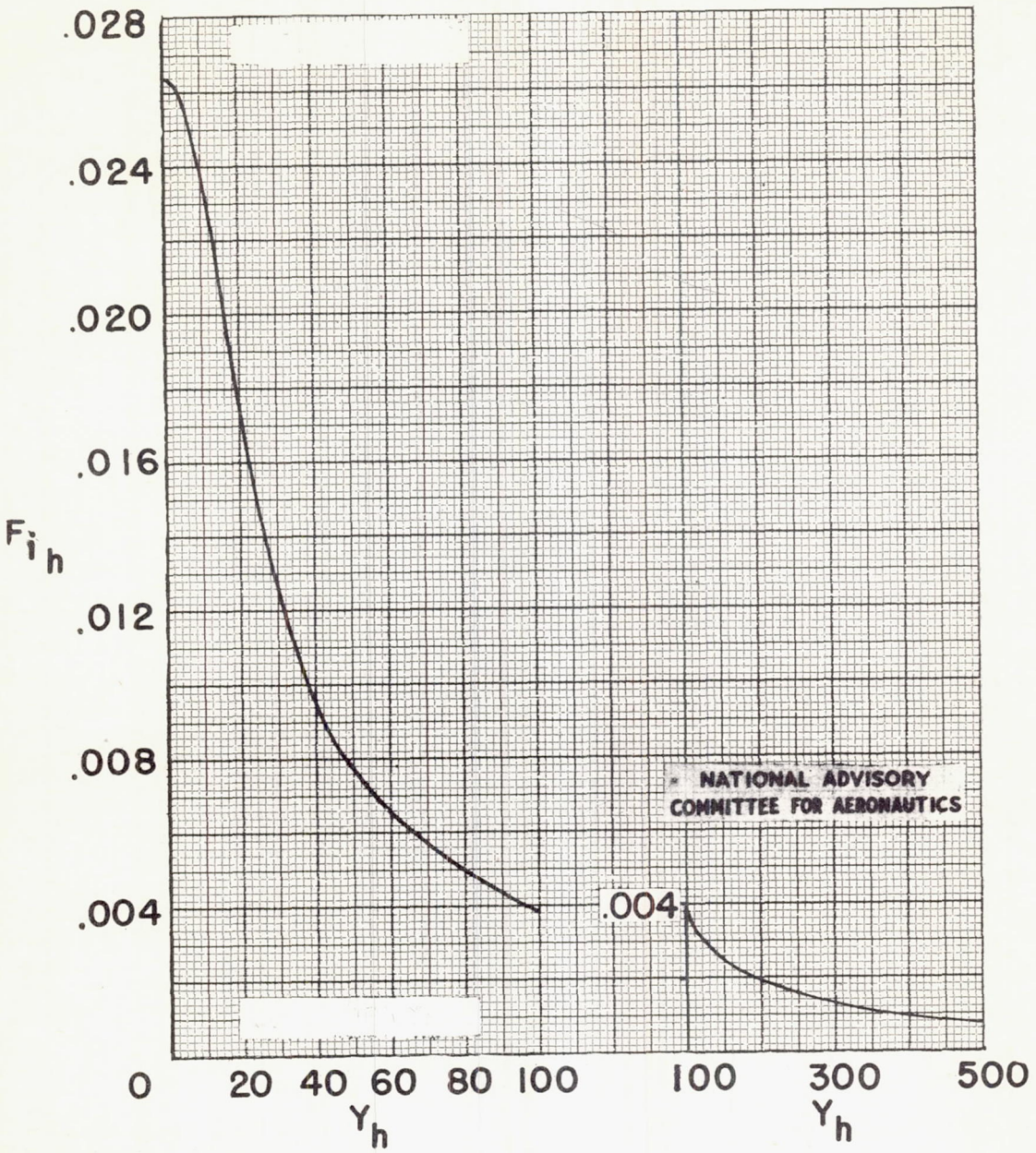

Figure 2.- Induced power-loading parameter in horizontal flight F_{i_h} against horizontal-speed parameter Y_h.

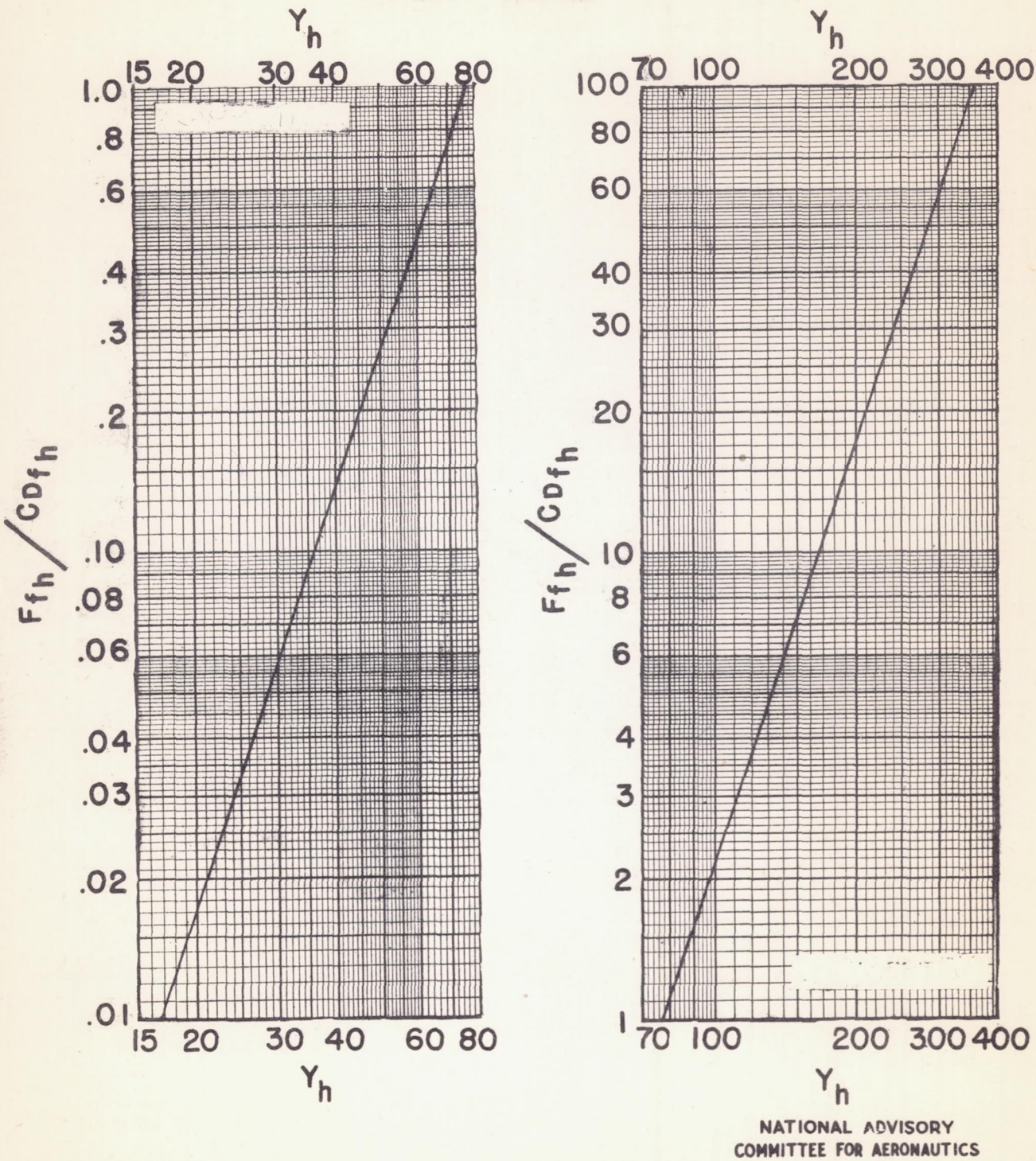

Figure 3.- Chart of $F_{f_h}/C_{D_{f_h}}$ against horizontal-speed parameter Y_h.

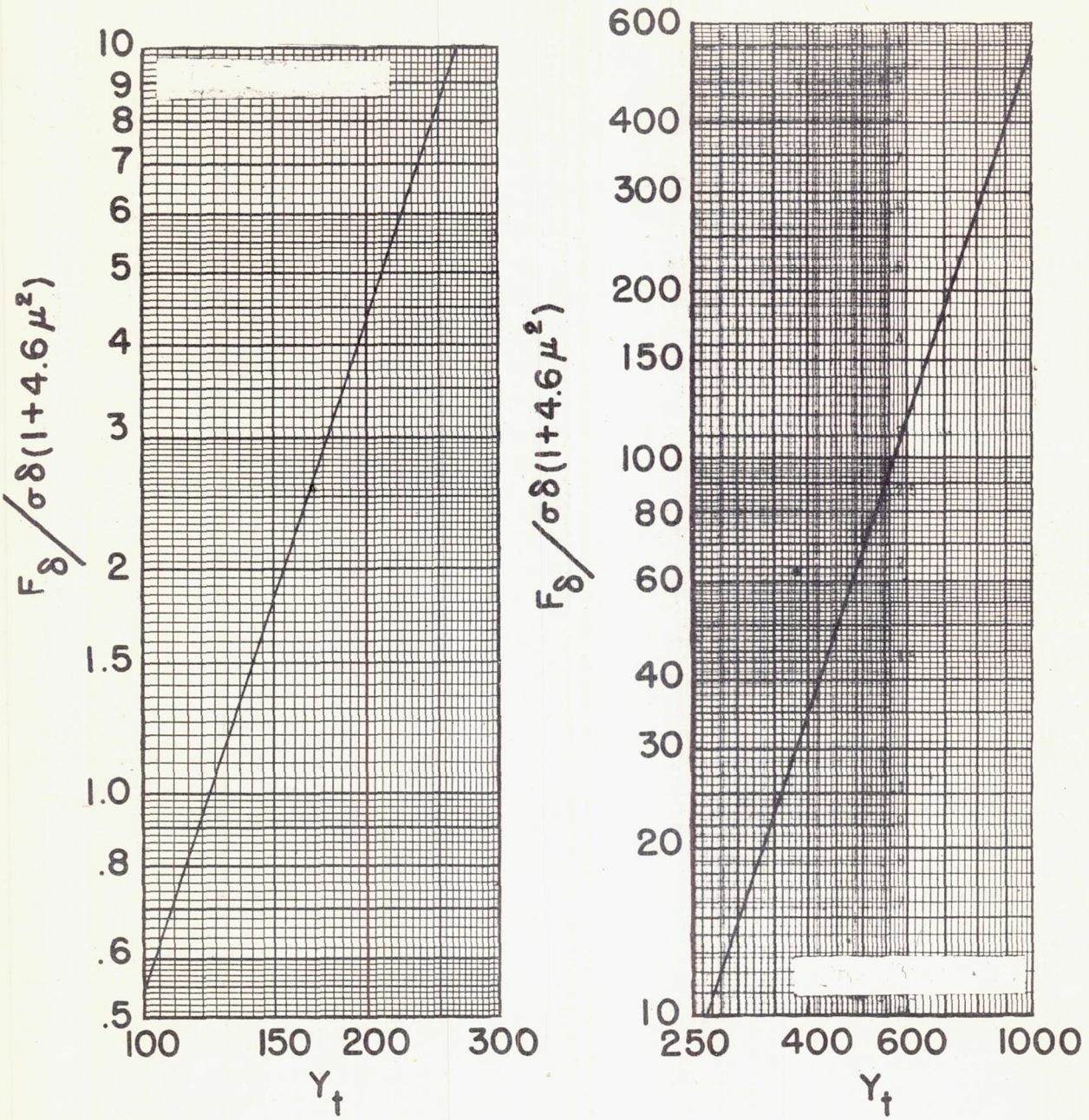

Figure 4.- Chart of $\frac{F_\delta}{\sigma\delta(1 + 4.6\mu^2)}$ against horizontal-speed parameter Y_h.

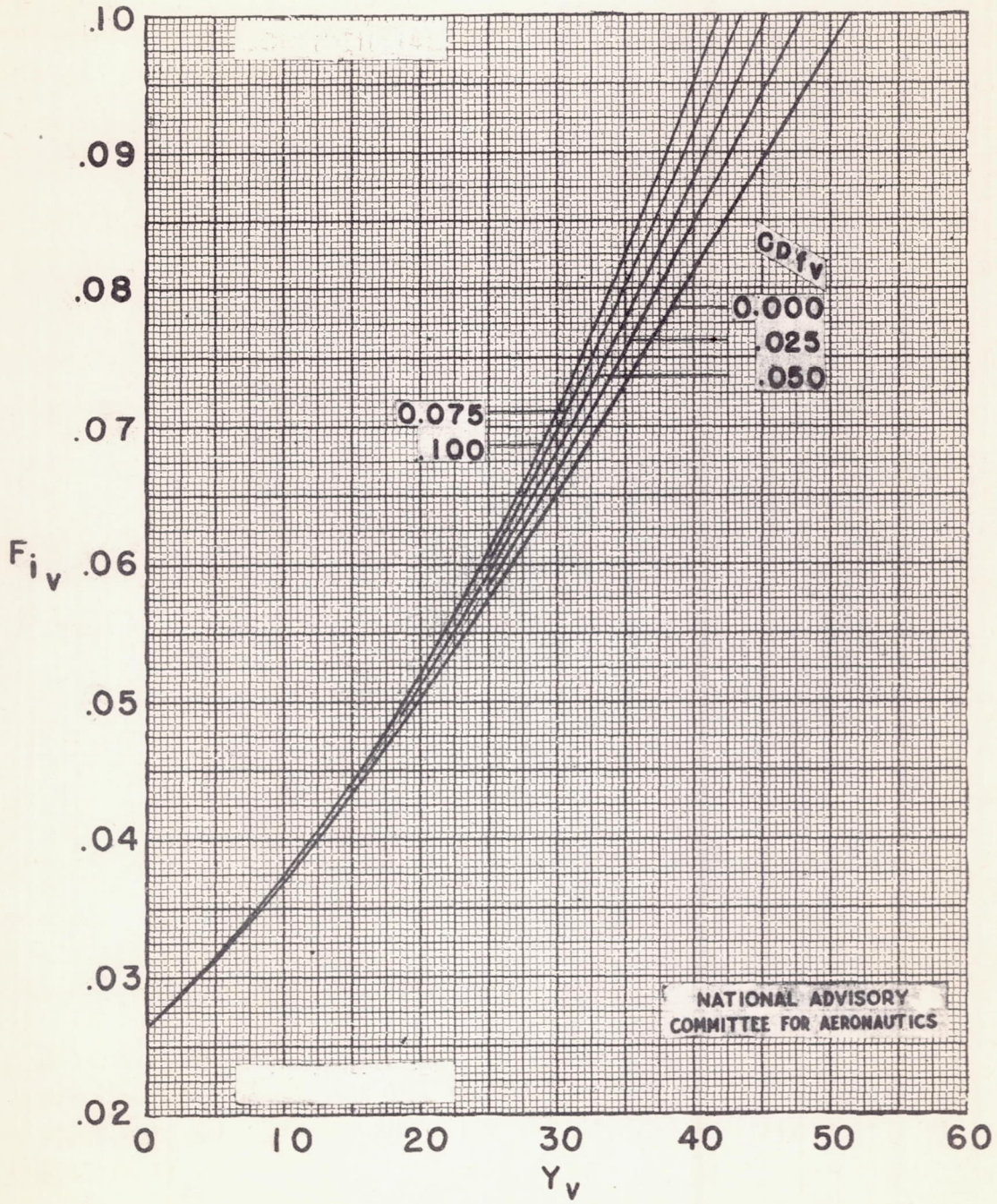

Figure 5.- Minimum induced power-loading parameter in vertical flight F_{i_v}. (For untwisted rectangular blades F_{i_v} is increased 6 percent.)

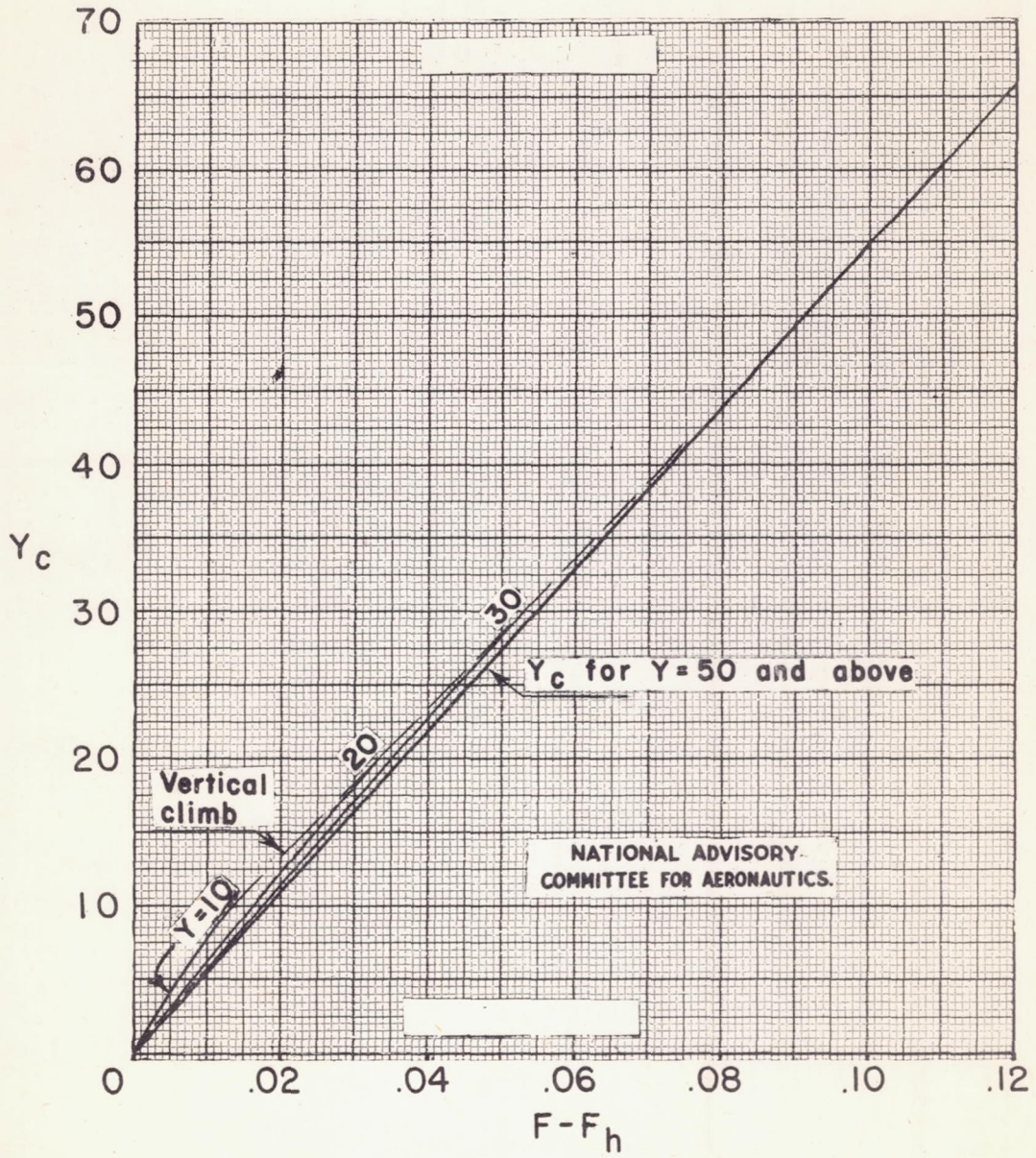

Figure 6.- Chart for finding the rate-of-climb parameter Y_c.

HOW TO USE FIGURE 7

In order to find the horizontal speed for maximum power loading, calculate $\sigma\delta Y_t$ where

σ rotor-disk equivalent solidity (For rectangular blades, $\sigma = \frac{bc}{\pi R}$ at $x = 1$; for other blade plan forms, $\sigma = 4\int_0^1 \sigma_x x^3 dx$)

δ rotor-blade average effective profile-drag coefficient

$Y_t = \Omega R\sqrt{\frac{A}{W}\frac{\rho}{\rho_0}}$ where ΩR = rotational tip speed, fps

Calculate $200\ C_{D_f}$ where

C_{D_f} helicopter drag coefficient in horizontal flight exclusive of rotor blades, based on rotor-disk area A

Lay a straight edge from the value of $\sigma\delta Y_t$ on the left-hand scale to the value of $\sigma\delta Y_t + 200\ C_{D_f}$ on the right-hand scale and read, as illustrated by the long dashed lines, the intersection with the solid curve on the scale of $Y_{best} = V\sqrt{\frac{A}{W}\frac{\rho}{\rho_0}}$, where V is the horizontal speed in feet per second for maximum power loading. In case the value of $\sigma\delta Y_t + 200\ C_{D_f}$ is greater than 0.6, read the vertical scales times 10 and use the short-dash curve to find Y_{best}.

The use of figure 7 is illustrated by a numerical example in section 8d. The equation of the figure is derived in section 5.

NATIONAL ADVISORY
COMMITTEE FOR AERONAUTICS

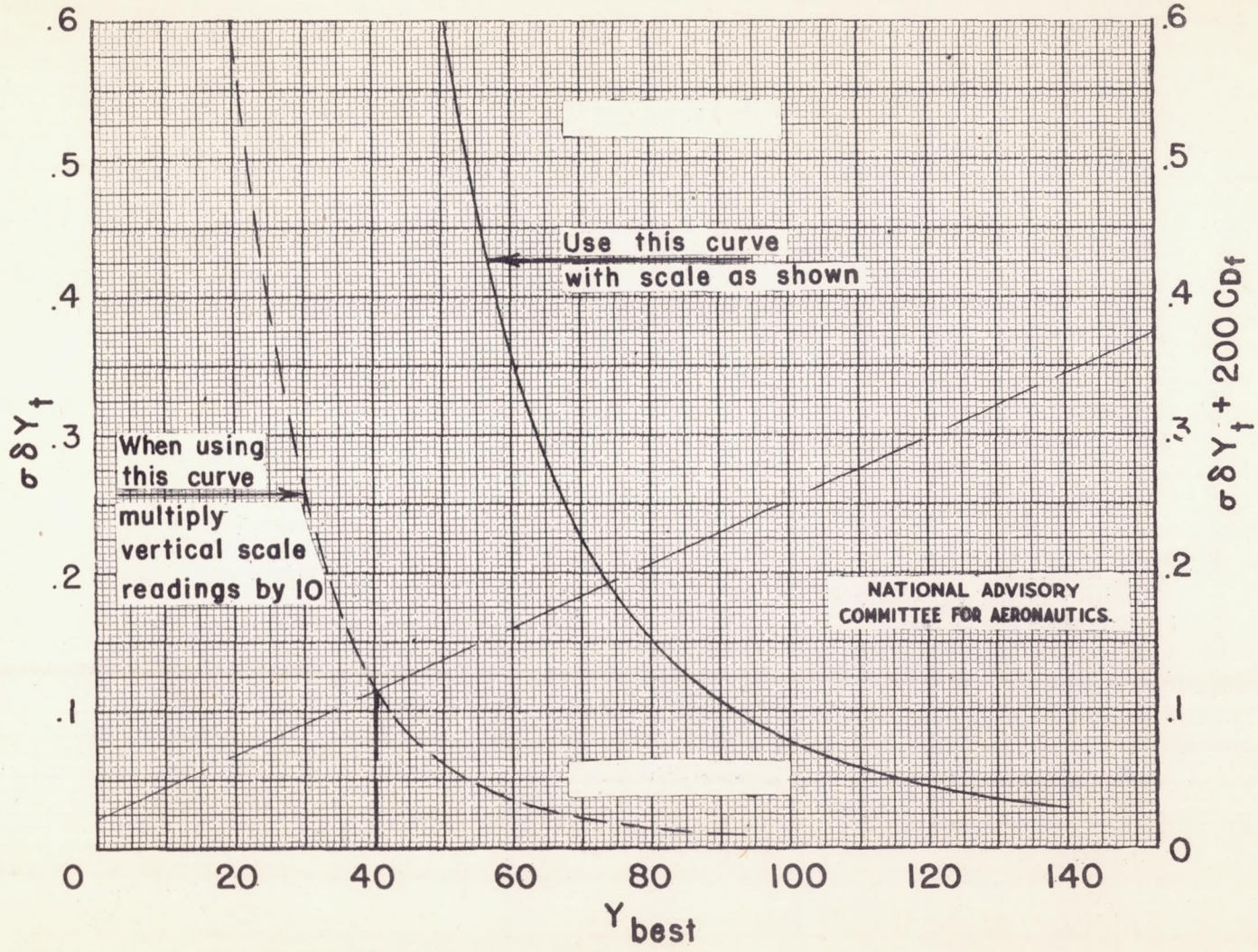

Figure 7.- Chart for finding the best-climbing-speed parameter Y_{best}.

HOW TO USE FIGURE 8

The solidity σ on the figure is for rectangular blades with a lift coefficient of 1.5 at the tip of the retreating blade in horizontal flight. The figure is read as follows:

Calculate $Y_h = V_h\sqrt{\frac{A}{W}\frac{\rho}{\rho_0}}$ where V_h is the horizontal speed in feet per second.

Calculate $\left(\frac{\sigma\delta}{\mu} + 2C_{D_{f_h}}\right)$ where

σ equivalent solidity $\left(\sigma = 4\int_0^1 \sigma_x x^3 dx\right)$

δ rotor-blade average effective profile-drag coefficient (see fig. 11)

μ ratio of the speed of the helicopter to the rotational tip speed of the rotor blades

$C_{D_{f_h}}$ helicopter drag coefficient in horizontal flight, exclusive of rotor blades, based on rotor-disk area A

Read the figure as shown by the dashed lines, entering the chart with the value of Y_h on the lower left-hand scale and from the curve of $\left(\frac{\sigma\delta}{\mu} + 2C_{D_{f_h}}\right)$ projecting upward to the curve of μ and reading the required value of σY_t^2 on the left-hand scale. Then, if the value of σ computed from σY_t^2 with the known value of $Y_t = \Omega R\sqrt{\frac{A}{W}\frac{\rho}{\rho_0}}$ is larger than the given σ, the blades are too narrow for a tip lift coefficient of 1.5. The value of σ required for a lift coefficient of 1.5 may be obtained by successive approximations.

The use of figure 8 is illustrated by a numerical example in section 8c. The equations of the figure are explained in section 6.

NATIONAL ADVISORY
COMMITTEE FOR AERONAUTICS

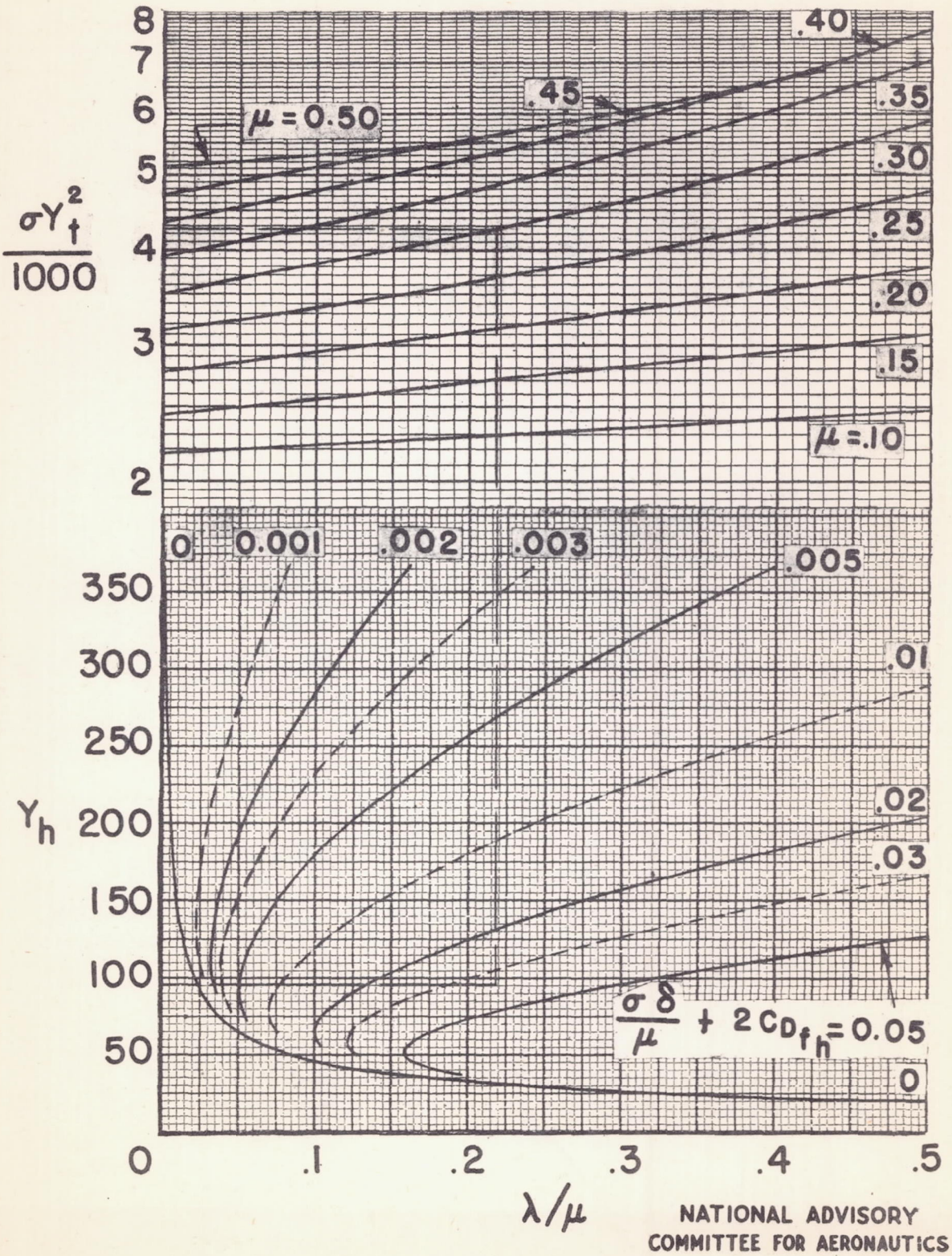

Figure 8.- Chart for determining the stalling limit σY_t^2 for untwisted rectangular blades.

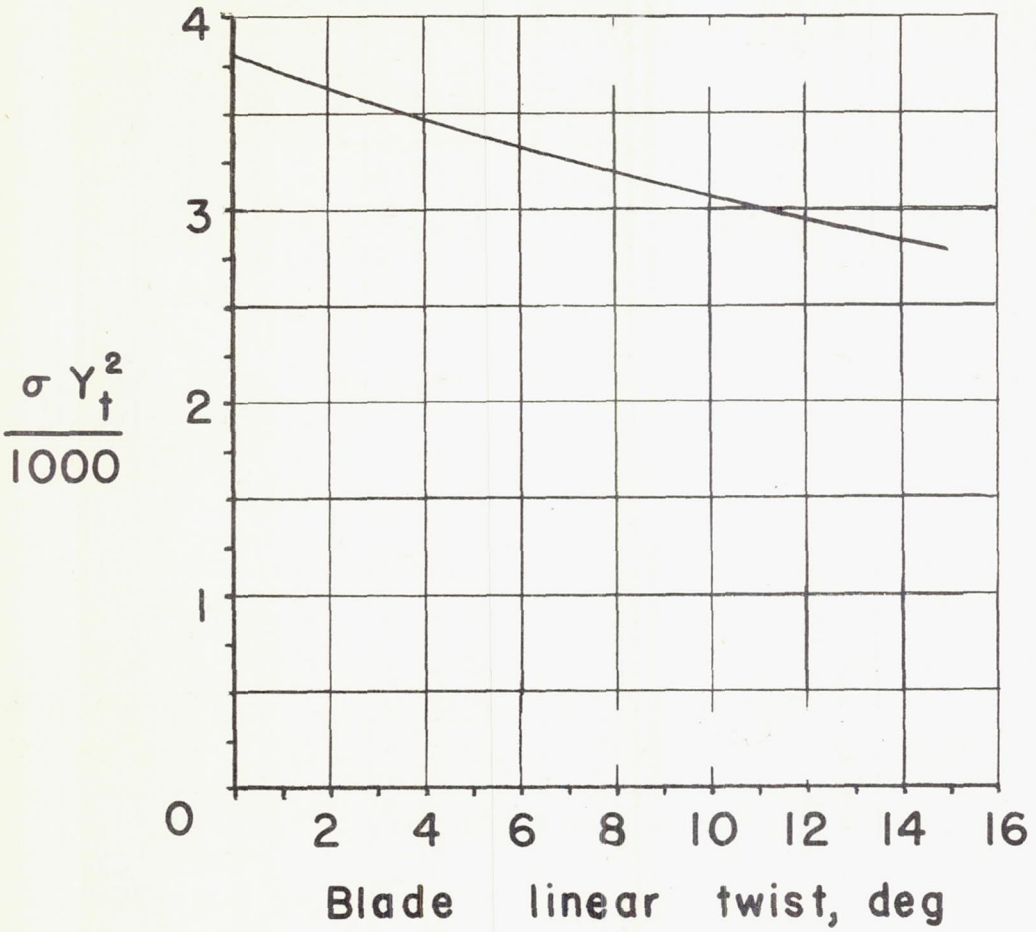

NATIONAL ADVISORY
COMMITTEE FOR AERONAUTICS

Figure 9.- The stalling limit σY_t^2 against blade linear twist for $\mu = 0.3$ and $\lambda = 0.03$.

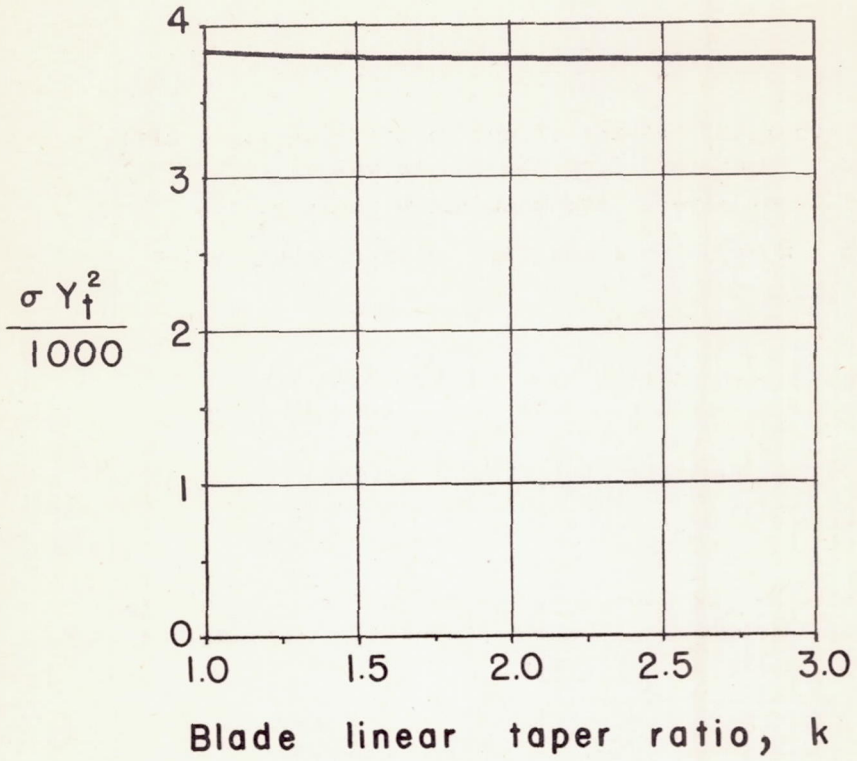

NATIONAL ADVISORY
COMMITTEE FOR AERONAUTICS

Figure 10.- The stalling limit σY_t^2 against blade linear taper for $\mu = 0.3$ and $\lambda = 0.03$.

HOW TO USE FIGURE 11

In order to find the effective profile-drag coefficient δ, first read from the figure values of $\sigma c_l Y_t^2$ and W.F. for several stations along the abscissa from $\left(\frac{\psi}{\pi} - \frac{1}{2}\right) = 0$ to 1 and for the appropriate value of μ, where

σ equivalent solidity $\left(\sigma = 4\int_0^1 \sigma_x x^3 dx\right)$

c_l rotor-blade-element lift coefficient

Y_t rotor tip-speed parameter $\left(Y_t = \Omega R \sqrt{\frac{A}{W}\frac{\rho}{\rho_0}}\right)$

μ ratio of the horizontal component of speed of the helicopter to the rotational tip speed of the rotor $\left(\mu = \frac{V \cos \alpha_1}{\Omega R}\right)$

From the known value of σY_t^2, compute c_l for each station selected. From the airfoil polar for the blade section at the 0.8 radius, read values of the profile-drag coefficient c_{d_o} corresponding to c_l and plot (W.F.) c_{d_o} against $\frac{\psi}{\pi} - \frac{1}{2}$ as illustrated in figure 13. The area under this curve is the value of δ.

The use of figure 11 is illustrated by a numerical example of section 8. The equations of the figure are explained in section 7a.

NATIONAL ADVISORY
COMMITTEE FOR AERONAUTICS

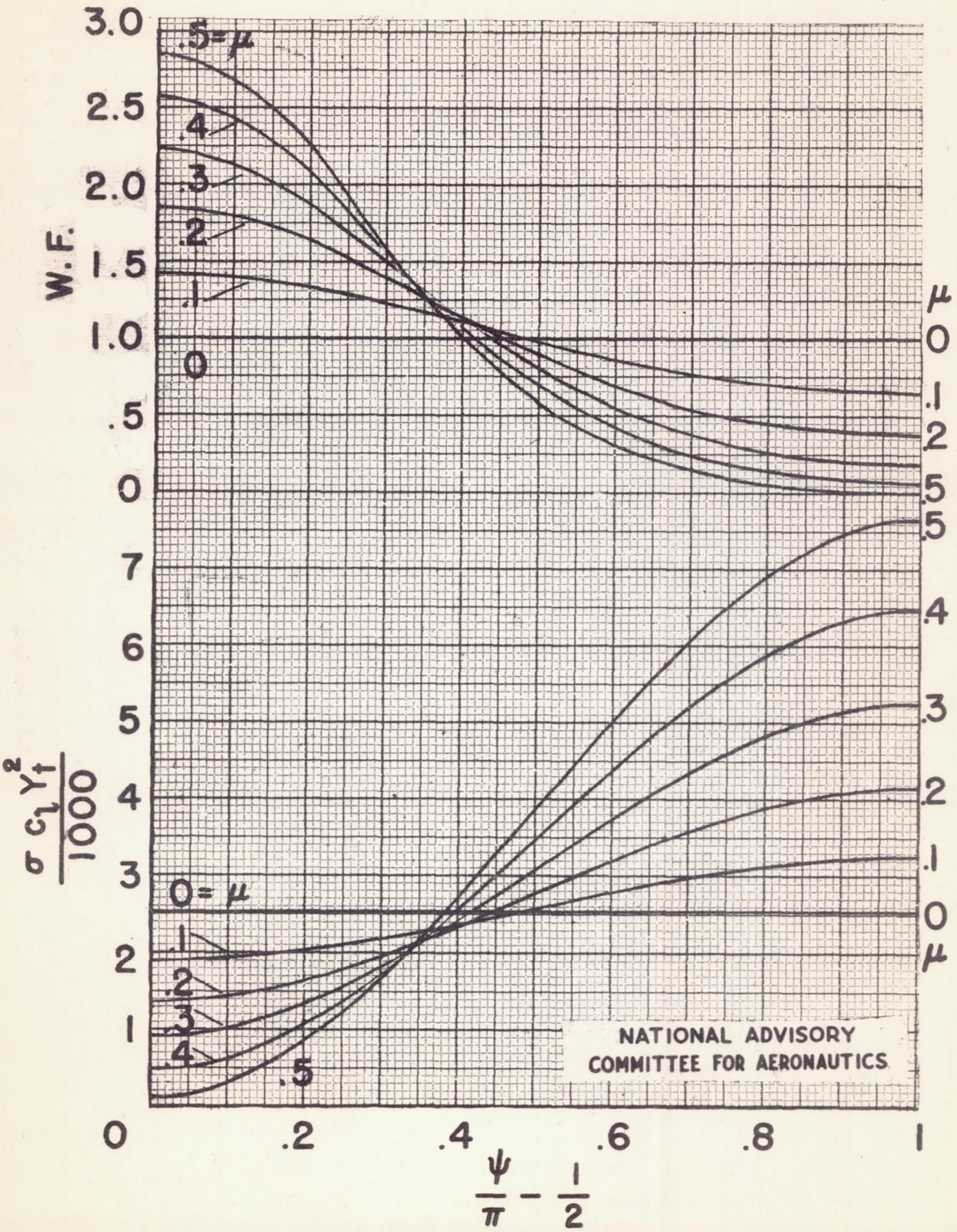

Figure 11.- Chart to be used in determining the effective blade profile-drag coefficient δ.

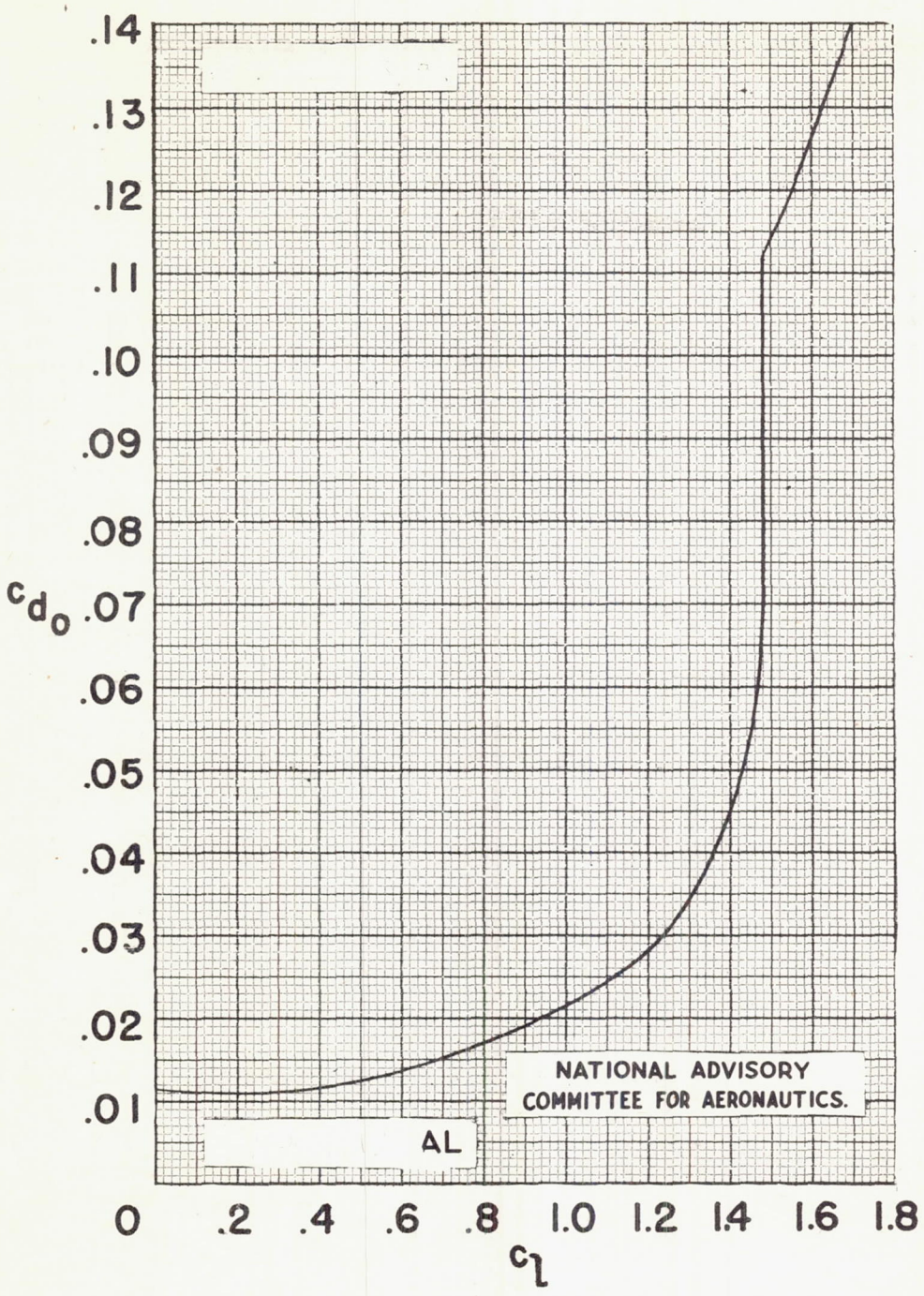

Figure 12.- Airfoil section profile-drag coefficient c_{d_o} against lift coefficient for rough conventional section (adapted from figure 1, reference 7, with a = 5.85).

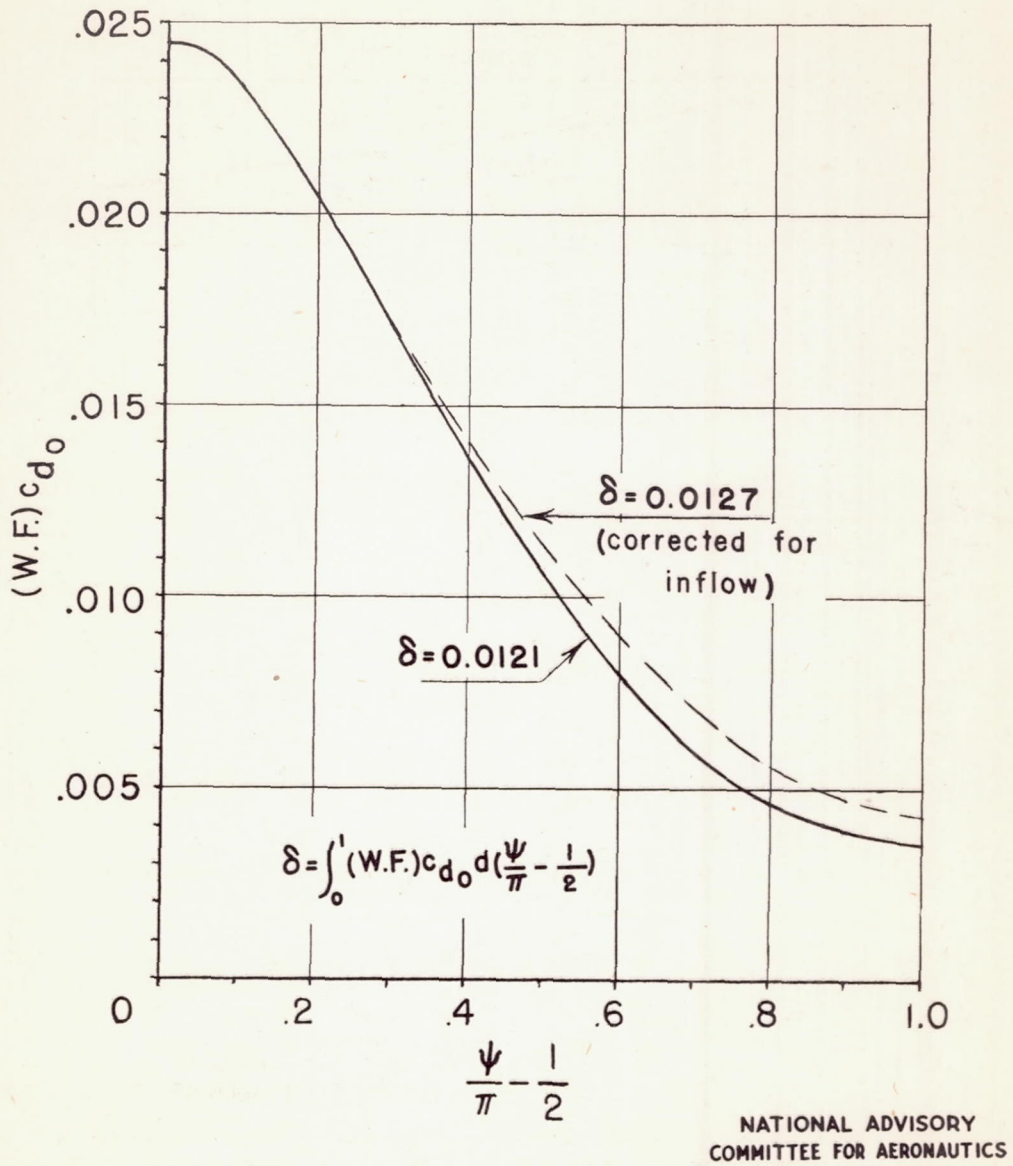

Figure 13.- Sample graph for finding δ. $\sigma Y_t^2 = 5740$; $\mu = 0.3$; airfoil polar from figure 12.

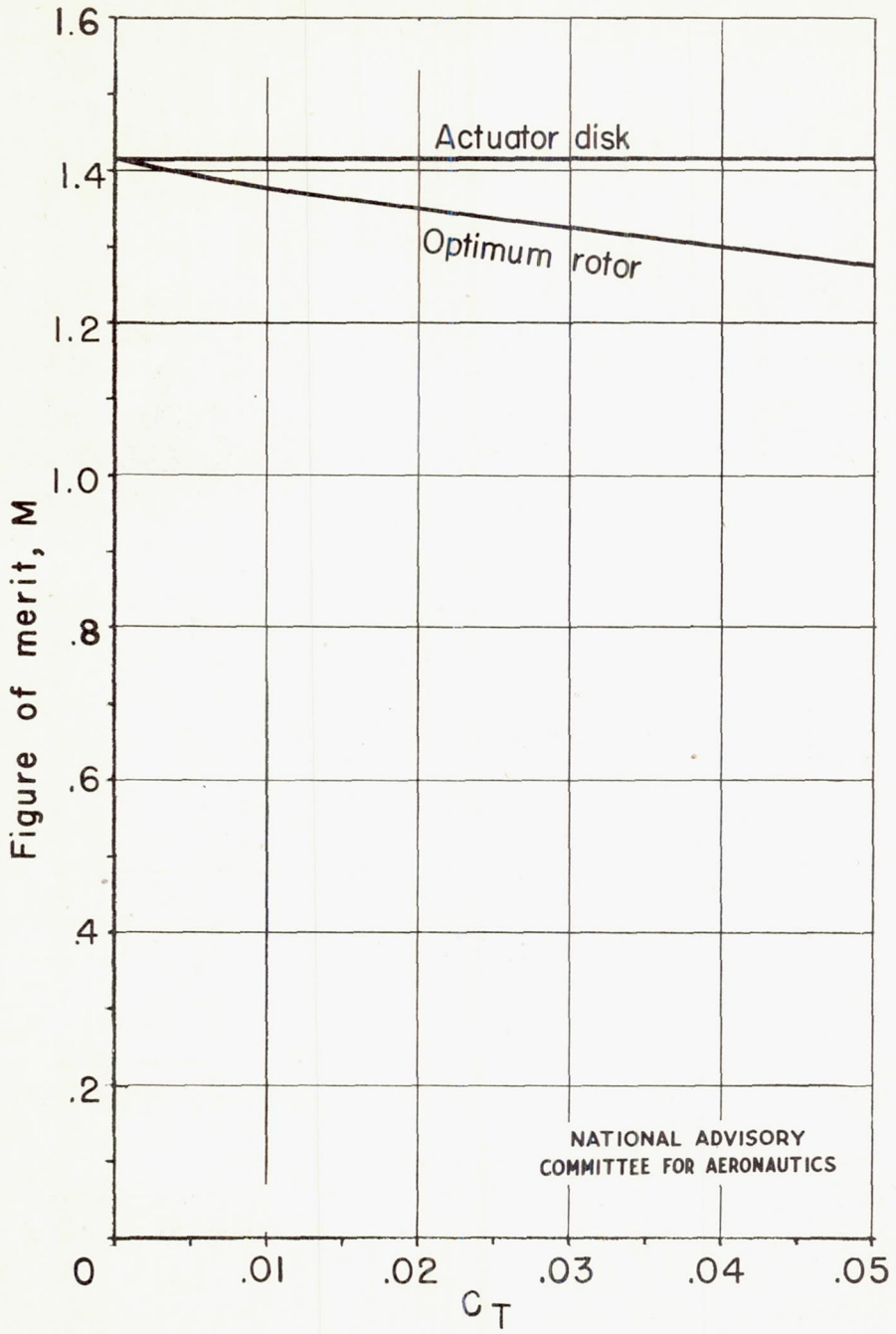

Figure 14.- Comparison of optimum rotor, without blade profile drag, with actuator disk. (From reference 2.)

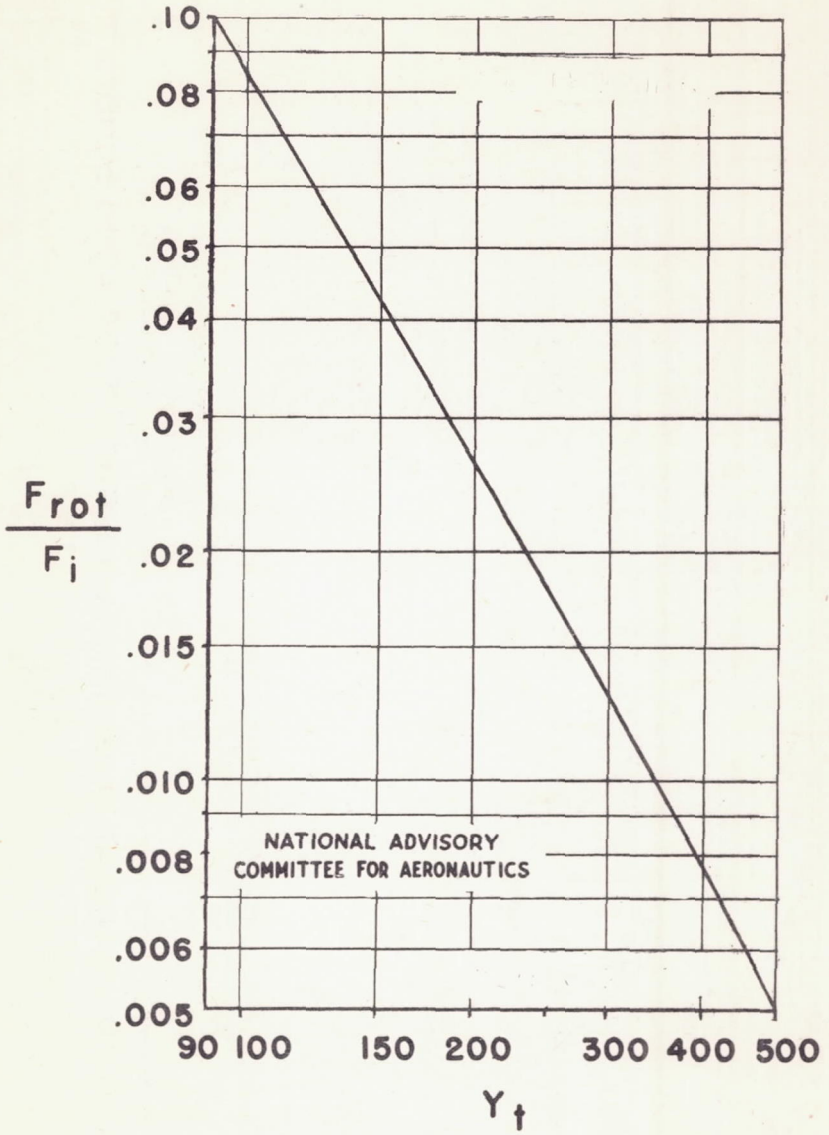

Figure 15.- Correction to F for slipstream rotation $\frac{F_{rot}}{F_i}$ against Y_t.

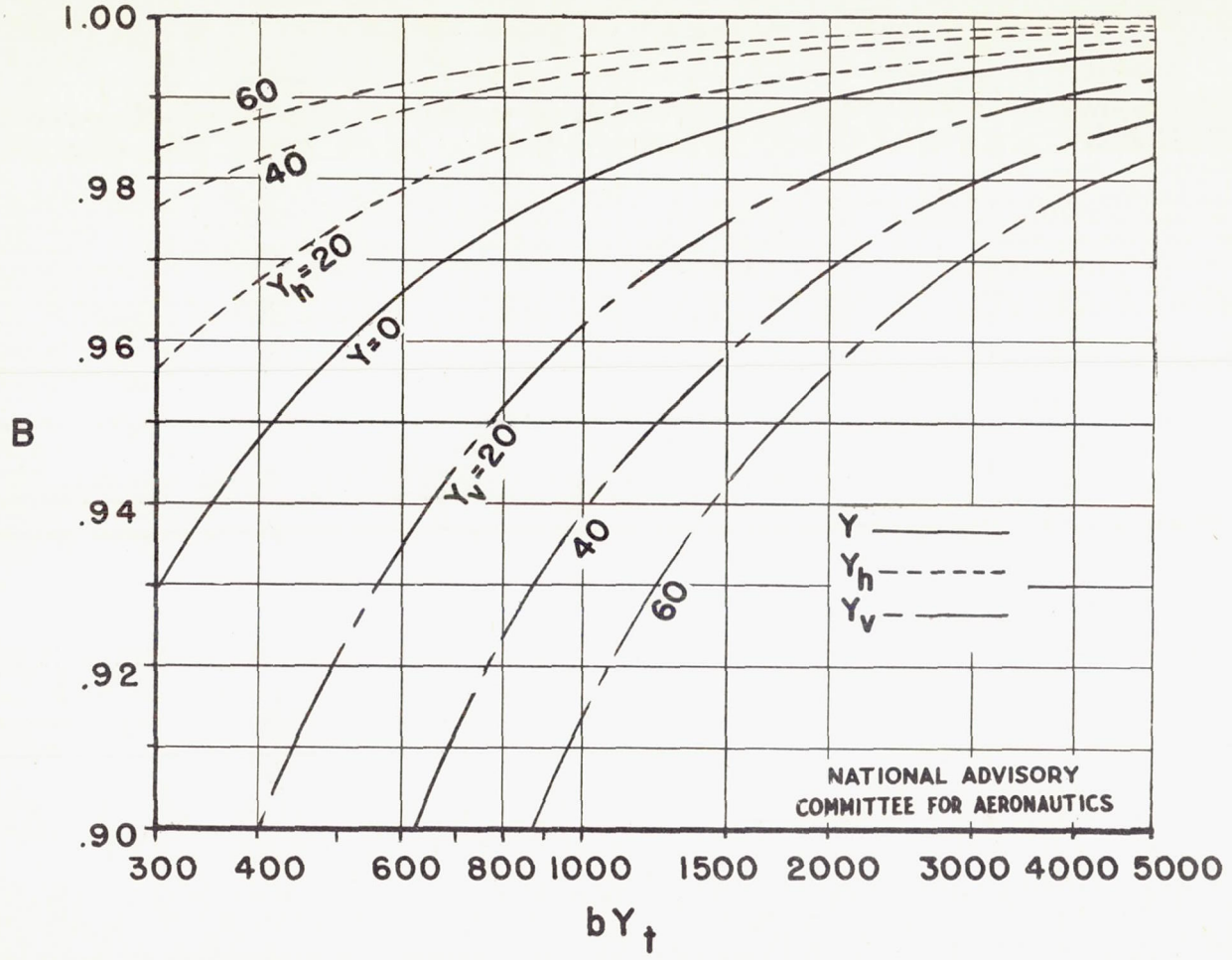

Figure 16.- Curves of B against bY_t for several values of Y_v and Y_h.

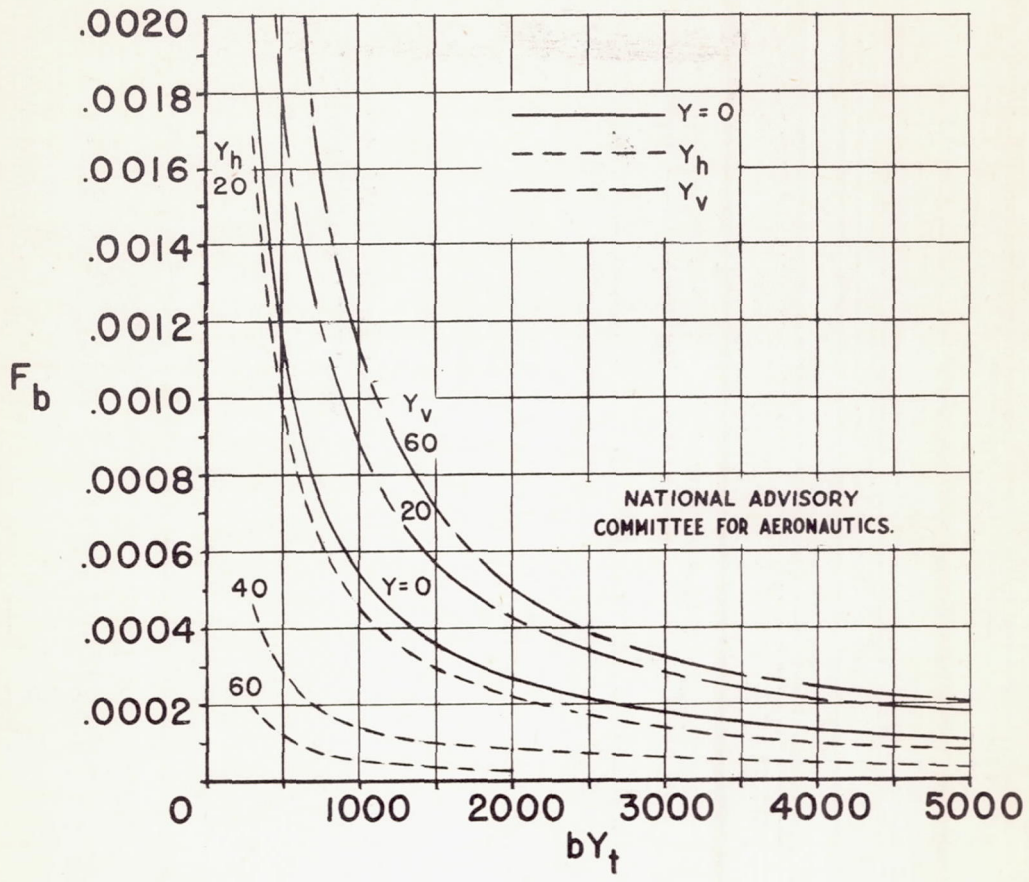

Figure 17.- Curves of the tip correction F_b against bY_t for horizontal flight, hovering, and several rates of vertical climb.

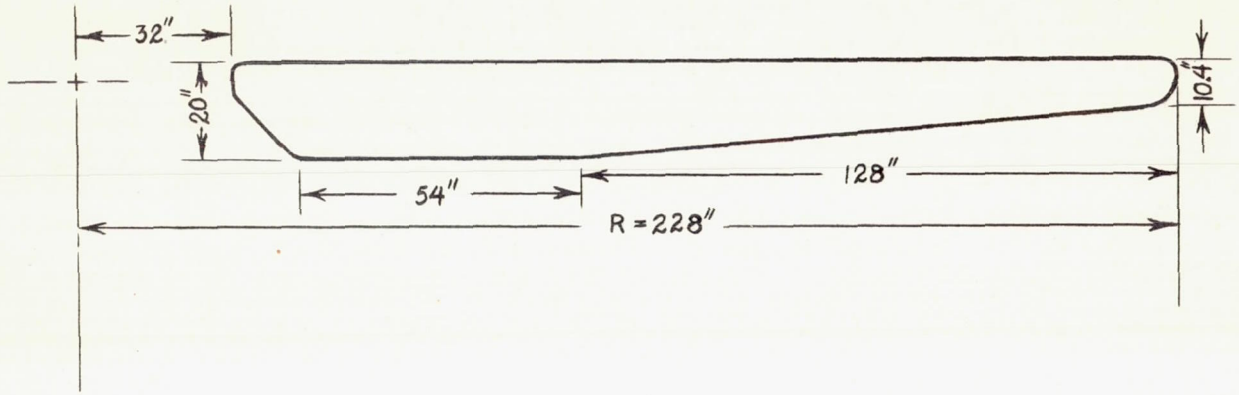

NATIONAL ADVISORY
COMMITTEE FOR AERONAUTICS

Figure 18.- Sketch of sample helicopter blade. Linear twist, 7°.